

**DEVELOPMENT OF SUB-CELLULAR  
ORGANELLE TARGETED FLUORESCENT  
SILICA NANOPARTICLES**

**A Thesis Submitted to  
the Graduate School of Engineering and Sciences of  
İzmir Institute of Technology  
in Partial Fulfillment of the Requirements for the Degree of**

**MASTER OF SCIENCE**

**in Chemistry**


**by  
Almila YÜKSEL**

**December 2019  
İZMİR**

We approve the thesis of **Almila YÜKSEL**

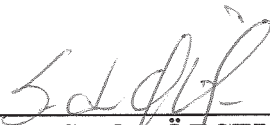
**Examining Committee Members:**

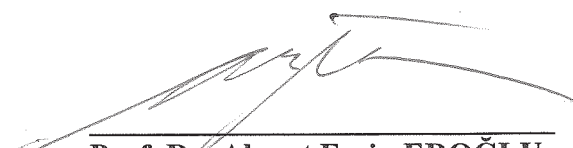
  
\_\_\_\_\_  
**Prof. Dr. Serdar ÖZÇELİK**  
Department of Chemistry, İzmir Institute of Technology

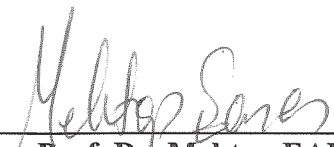
  
\_\_\_\_\_  
**Prof. Dr. Gülşah ŞANLI MOHAMED**  
Department of Chemistry, İzmir Institute of Technology

  
\_\_\_\_\_  
**Prof. Dr. Şerife Esra ERDAL BAĞRIYANIK**  
Department of Medical Biology and Genetics, Dokuz Eylul University

**20 December 2019**

  
\_\_\_\_\_  
**Prof. Dr. Serdar ÖZÇELİK**  
Supervisor,  
Department of Chemistry  
İzmir Institute of Technology

  
\_\_\_\_\_  
**Prof. Dr. Ahmet Emin EROĞLU**  
Head of the Department of Chemistry

  
\_\_\_\_\_  
**Prof. Dr. Mehtap EANES**  
Dean of the Graduate School of  
Engineering and Science

## ACKNOWLEDGMENTS

First of all, I wish to express my sincere appreciation to my advisor Prof. Dr. Serdar Özçelik for his invaluable comments, suggestions and sharing of knowledge to make this study more meaningful.

I would also express my warmest gratitude to Dr. Özge Tuncel for her guidance and countless help I have received. Besides, I would like to thanks to my colleagues Dr. Seçil Sevim Ünlütürk, Dr. Melek Özkan Üçüncü, Eylem Kurulgan and İlayda Melek Yırtıcı for their frequent helps and friendships. It is a pleasure to thank my lovely friend and colleague Hande Uçak who has always been a major source of support when things would get a bit discouraging.

My very special thanks goes to my aunt Seval Köylü, aunt's husband Fatih Köylü and my cousin Kemal Köylü for keeping me always in their hearts, thoughts and prayers.

Last but not least, I am truly grateful to my family, in particular, my mother Nilgün Demirel and my father İlker Yüksel for their immeasurable love and care. I would like to dedicate this work to my mother whose dreams for me have resulted in this achievement and without her loving upbringing; I would not have been where I am today and what I am today.

# ABSTRACT

## DEVELOPMENT OF SUB-CELLULAR ORGANELLE TARGETED FLUORESCENT SILICA NANOPARTICLES

Silica nanoparticles have been studied extensively in cellular applications due to their physicochemical properties. The surface of silica nanoparticles represent the key parameter in biological studies. Owing to their versatile surface chemistry, have ability to increase bioavailability and selectivity. Therefore, it is significant to understand how biomolecules interact with the surface of silica nanoparticles.

The study reviews how synthesized both negative and positive potential silica nanoparticles and can transfer their properties to the cells. In the second part, our synthesized silica nanoparticles were characterized physicochemically using some instrumental devices. To answer the role of silica nanoparticles in the cells, some outcomes such as viability test, image analysis, colocalization analysis and mitochondrial membrane potential were investigated. A549 (adenocarcinomic human alveolar basal epithelial cells) and BEAS-2B (human bronchial epithelial cells) cell lines were selected in our studies.

Our results showed the cytotoxicity was dose and time dependent in direct proportion. Mitochondrial accumulation were observed in cells treated with the silica nanoparticles according to Pearson's Coefficient Correlation and Image J analysis.

The study concluded that the silica nanoparticles can be used in the field of targeted delivery and bioimaging in cellular studies.

## ÖZET

### HÜCRE-ALTI ORGANEL HEDEFLİ FLORESAN SİLİKA NANOTANECİKLERİN GELİŞTİRİLMESİ

Nanotaneçikler fizikokimyasal özellikleri sebebiyle hücresele çalıřmalarda çok tercih edilmektedir. Silika nanotaneçiklerin yüzey kimyası deęiřtirilerek biyolojik çalıřmalarda uygulanabilir hale getirilebilir. Çok yönlü yüzey kimya platformuna sahip olmaları nedeniyle, biyoyararlanımı ve seçicilięi arttırma yeteneęine sahiptir. Bu nedenle, biyomoleküllerin silika nanoparçacıkların yüzeyi ile nasıl etkileřime girdięini anlamak önemlidir.

Bu çalıřma hem negatif yüklü hem de pozitif yüklü silica nanoparçacıkların nasıl sentezlendięini ve özelliklerini hücrelere nasıl aktardıklarını inceler. İkinci kısımda, sentezlenen iki farklı silika nanotaneçięin karakterizasyonu enstrümental analiz cihazlar yardımıyla tayin edilmiřtir. Silica nanotaneçiklerin hücredeki davranıřını öğrenmek için canlılık testi, görüntü analizi, kolokalizasyon analizi ve mitokondri potansiyel ölçümü gibi deneyler yapılmıřtır. Bu amaçla çalıřmalarımızda A549 ve BEAS-2B hücre hatları seçilmiřtir.

Çalıřmalarımız göstermektedir ki, sentezlenen silika nanotaneçikler doz ve zamana doęrudan baęlı olarak sitotoksositeye etki etmektedir. Pearson Korelasyon Katsayısı ve Image J analiz sonuçlarına göre, sentezlenen silika nanotaneçiklerin hücrede mitokondri içerisinde biriktięi gözlemlenmiřtir.

Sonuç olarak, silica nanotaneçiklerin hedefe yönelik taşıyıcı uygulamalarda veya biyogörüntülemelemede kullanılmaları beklenmektedir.

# TABLE OF CONTENTS

LIST OF FIGURES .....	viii
LIST OF TABLES .....	xi
CHAPTER 1. INTRODUCTION .....	1
CHAPTER 2. SYNTHESIS AND SURFACE FUNCTIONALIZATION OF FLUORESCENT SILICA NANOPARTICLES.....	14
2.1. Introduction .....	14
2.2. Experimental .....	18
2.2.1. Chemicals and Reagents .....	18
2.2.2. Instrumentation .....	19
2.2.3. Synthesis of (-) Potential Silica Nanoparticles .....	19
2.2.4. Synthesis of (+) Potential Silica Nanoparticles .....	21
2.3. Results and Discussion .....	23
2.3.1. Characterization of (-) and (+) Silica Nanoparticles.....	23
2.4. Conclusion .....	32
CHAPTER 3. PARTICLE-CELL INTERACTION .....	33
3.1. Introduction .....	33
3.1.1. Cell Lines .....	33
3.1.2. Cell Viability .....	35
3.1.3. Staining of Mitochondria .....	36
3.1.4. Mitochondrial Membrane Potential .....	36
3.1.5. Confocal Microscopy .....	37
3.1.6. Colocalization Analysis .....	39
3.2. Experimental .....	39
3.2.1. Materials .....	39
3.2.2. Instrumentation .....	40

3.2.3. Cell Cultivation .....	40
3.2.4. Cell Imaging .....	40
3.2.5. Cytotoxicity .....	41
3.3. Results and Discussion .....	42
3.3.1. MTT Assay .....	42
3.3.2. Confocal Imaging .....	44
3.3.3. Colocalization Analysis .....	48
3.3.4. Mitochondrial Intensity Analysis .....	50
3.4. Conclusion .....	51
CHAPTER 4. CONCLUSION .....	53
REFERENCES .....	54

## LIST OF FIGURES

<u>Figure</u>	<u>Page</u>
Figure 1.1. Nanoscale of objects <sup>1</sup> .....	1
Figure 1.2. Schematic diagram of different types of nanomaterials <sup>3</sup> .....	2
Figure 1.3. Mechanism of Microemulsion silica nanoparticles <sup>5</sup> .....	3
Figure 1.4. Mechanism of Stöber silica nanoparticles <sup>5</sup> .....	4
Figure 1.5. Hydrolysis and Condensation reactions of TEOS.....	5
Figure 1.6. Jablonski diagram process within fluorophore <sup>13</sup> .....	6
Figure 1.7. Commonly used functional groups binding different nanoparticles <sup>19</sup> .....	8
Figure 1.8. Confocal laser scanning microscope images of (a) Hela cells and (b) HepG2 cell lines with MSNP both coated with NH <sub>2</sub> and PPh <sub>3</sub> <sup>27</sup> .....	9
Figure 1.9. Confocal microscope images of MDA-MB-468 cell lines and mesoporous silica NPs with different sizes. (A) 190 nm, (B) 420 nm and (C) 1220 nm <sup>28</sup> .....	11
Figure 2.1. Absorption and fluorescence spectrum of FITC <sup>40</sup> .....	15
Figure 2.2. Electromagnetic spectrum <sup>44</sup> .....	17
Figure 2.3. Summary of (a) bare silica nanoparticles and (b) structures of FITC-APTES conjugate molecule.....	20
Figure 2.4. Preparation procedure of (-) potential silica nanoparticles.....	21
Figure 2.5. Summary of (a) structures of TMAC molecule, (b) schematic representation of potential silica nanoparticles.....	22
Figure 2.6. Preparation procedure of (+) potential silica nanoparticles.....	22
Figure 2.7. The sized of the (-) SiNPs and (+) SiNPs.....	23
Figure 2.8. The zeta potentials of the (-) SiNPs and (+) SiNPs.....	24
Figure 2.9. The absorption and PL spectra of silica nanoparticles.....	24
Figure 2.10. The pH dependence of fluorescence intensity of free FITC.....	25
Figure 2.11. The pH dependence of fluorescence intensity of silica nanoparticles.....	25
Figure 2.12. Solvent effect: fluorescence intensity of free FITC.....	26
Figure 2.13. Solvent effect: fluorescence intensity of silica nanoparticles.....	26
Figure 2.14. Stern-Volmer plot of quenching effect for both free FITC and silica nanoparticles in the presence of quencher I <sup>-</sup> .....	27



<b><u>Figure</u></b>	<b><u>Page</u></b>
Figure 2.15. Stern-Volmer plot of quenching effect for free FITC in the presence of quencher $\text{Cu}^{2+}$ .....	28
Figure 2.16. Stern-Volmer plot of quenching effect for silica nanoparticles in the presence of quencher $\text{Cu}^{2+}$ .....	28
Figure 2.17. FTIR spectra of (-) and (+) potential silica nanoparticles.....	29
Figure 2.18. STEM images of dark field of (-) SiNPs (a) in 50.000 magnification, (b) in 100.000 magnification and (c) 200.000 magnification, bright field of (-) SiNPs (d) in 100.000 magnification.....	30
Figure 2.19. SEM images of (+) SiNPs (a), (b) in 200.000 magnification.....	31
Figure 3.1. Morphology of (a) A549 and (b) BEAS-2B at low density and high density <sup>53</sup> .....	33
Figure 3.2. Statistics of cancer types for new cases diagnosed in Turkey, 2018 <sup>56</sup> .....	35
Figure 3.3. Enzymatic reduction of MTT to formazan.....	35
Figure 3.4. The diagram of mitochondrial membrane potential <sup>62</sup> .....	37
Figure 3.5. Laser scanning confocal microscopy set-up <sup>65</sup> .....	38
Figure 3.6. Spinning disk confocal microscopy set-up <sup>67</sup> .....	38
Figure 3.7. The schematic representation of MTT assay of (a) (-) SiNPs and (b) (+) SiNPs for A549 cell line.....	42
Figure 3.8. The schematic representation of MTT assay of (a) (-) SiNPs and (b) (+) SiNPs for BEAS-2B cell line.....	43
Figure 3.9. Confocal images of control group for (a) A549 cell line and (b) BEAS-2B cell line using 100x objective.....	44
Figure 3.10. Confocal images of (-) SiNPs-treated with A549 cell line for (a) 40x objective and (b), (c) 100x objective.....	45
Figure 3.11. Confocal images of (+) SiNPs-treated with A549 cell line for (a) 40x objective and (b), (c) 100x objective.....	46
Figure 3.12. Confocal images of (-) SiNPs-treated with BEAS-2B cell line for (a) 40x objective and (b), (c) 100x objective.....	47
Figure 3.13. Confocal images of (+) SiNPs-treated with BEAS-2B cell line for (a) 40x objective and (b), (c) 100x objective.....	47

<b><u>Figure</u></b>	<b><u>Page</u></b>
Figure 3.14. Distribution of pearson coefficients of (-) SiNPs, (+) SiNPs and Control group for A549 and (b) BEAS-2B cell.....	49
Figure 3.15. Mitochondrial intensity analysis of (-) SiNPs, (+) SiNPs and Control group for A549 cell line.....	50
Figure 3.16. Mitochondrial intensity analysis of (-) SiNPs, (+) SiNPs and Control group for BEAS-2B cell line.....	51

## LIST OF TABLES

<b><u>Table</u></b>	<b><u>Page</u></b>
Table 1.1. Toxicity of SiNPs according to literature studies.....	12
Table 2.1. Infrared spectra of some common functional groups.....	17
Table 2.2. Energy Dispersive X-Ray Spectroscopy analysis of (-) SiNPs.....	30
Table 2.3. Energy Dispersive X-Ray Spectroscopy analysis of (+) SiNPs.....	31
Table 3.1. Statistics of common types of cancer globally <sup>55</sup> .....	34

# CHAPTER I

## INTRODUCTION

### 1.1. Nanotechnology and Nanomaterials

Nanotechnology and nanoscience is the emerging science of molecules and atoms in the range of approximately 0.1-100nm. In Figure 1.1., nanometer scale was given with the help of some objects.<sup>1</sup> The background of nanotechnology first came from by Richard Feynman, physicist entitled “There’s Plenty of Room at the Bottom”. He stated that the ability to utilize materials on a atomic scale could be very interesting.

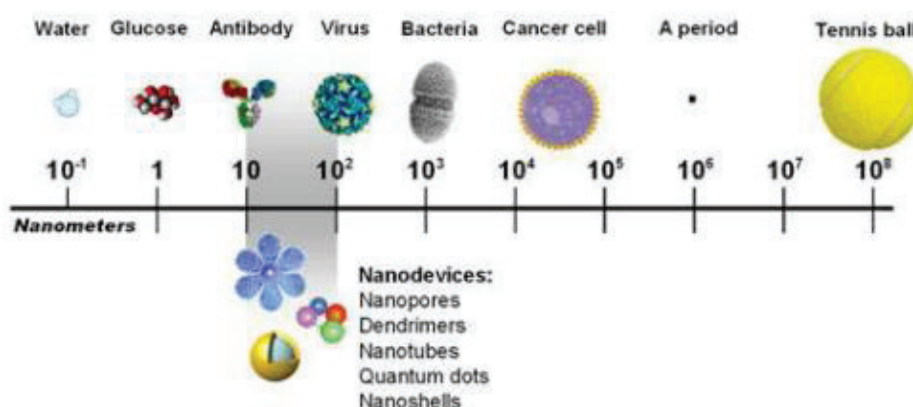


Figure 1.1. Nanoscale of objects.<sup>1</sup>

Nanotechnology has rapidly expanding field over the past 20 years. Nanotechnology is the area of science disciplines that make use of design, characterization and production of materials at nano scale. The impact of nanoscience disciplines are often generating enhanced materials in order to make solar power more economical, surgeries could become much faster or nanobots could help construct materials. Besides, smaller and faster electronic devices or more accurate medical diagnostic equipment can be possible in a way of nanotechnology. This illustrates that the nanotechnology has many potential applications as follows energy, healthcare,

electronic and many more. It can be concluded that nanotechnology has play an important role in our lives.

Nanomaterials have novel characteristic compared to bulk material which is not exhibit nanoscale features. The two reasons why nanomaterials have significant changes in chemical, mechanical and optical properties are increased surface area and new quantum effects. In other words, surface to volume ratio increases and properties of materials become size dependent. When the size of particle decreases greater proportion of atoms are placed at the surface rather than inside. This means the nanoparticles form will be much more reactive. They often have unique properties because they have their own physical and chemical properties. Using nanomaterials promise certain advantages on a daily lives in terms of get low cost and high quality products.<sup>2</sup>

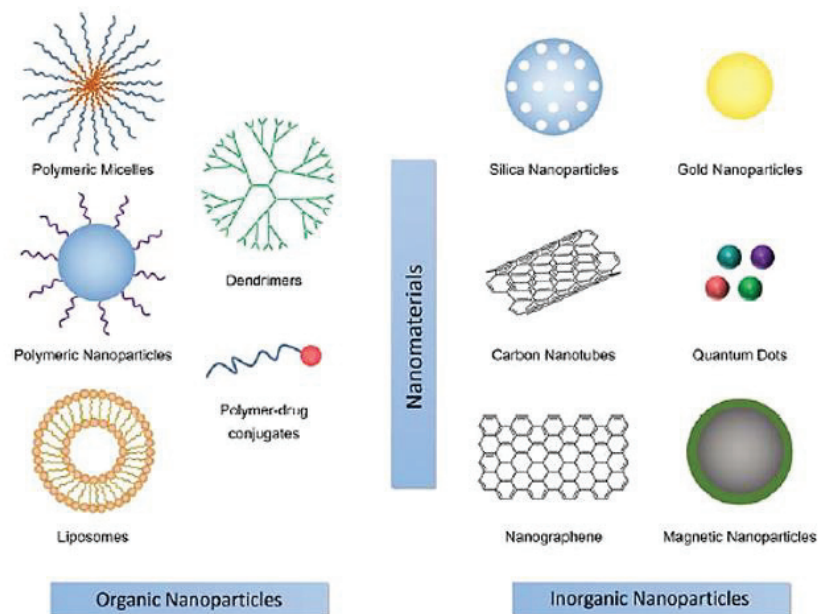


Figure 1.2. Schematic diagram of different types of nanomaterials.<sup>3</sup>

Nanomaterials are the products of nanotechnology that shown in Figure 1.2.<sup>3</sup> Some of them occur naturally, but the certain interest are synthesized nanomaterials, which can be used in many commercial processes. Organic nanoparticles can be classified into nanomaterials such as polymeric nanoparticles, liposomes and dendrimers. Apart from that materials, inorganic nanomaterials have been widely

explored especially in biomedicine, for example, silica nanoparticles, gold nanoparticles and quantum dots.

Silica nanoparticles are the example of inorganic nanoparticles. Silicon dioxide or silica is commonly found in nature as forms of quartz, opal etc. It is the second-most common element in terms of Earth's crust. SiO<sub>2</sub> was first discovered by Jons Berzelius who Swedish chemist in 1824. Silica nanoparticles have attracted great interest due to the fact of their physical properties including nontoxicity, biocompatibility and scalable synthetic availability.<sup>4</sup> Silica has both bulk and nano form for many years. For example, bulk form of silica has been used as a food additive and anti-foaming agent. Nano-silica is being developed for biomedical studies such as drug delivery and cancer therapy. In order to produce nano form of silica, Stöber and Microemulsion concerning the mostly applied methods in many academic laboratories. The methodologies of these methods were indicated. (Figure 1.3-4.)<sup>5</sup> Microemulsion method includes water, oil which are immiscible mixture stabilized with the aid of surfactant. This method can be made as water-in-oil or oil-in-water concerning the surfactant. Large concentration of surfactant and co-surfactant are needed to enable synthesis of nanoparticles.

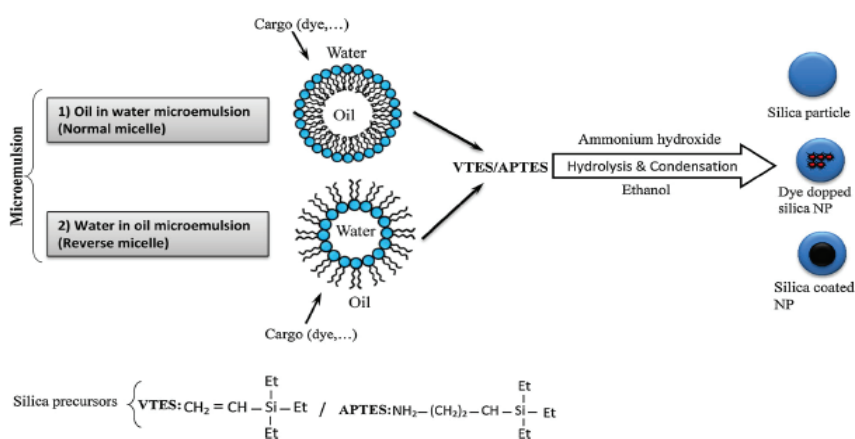


Figure 1.3. Mechanism of Microemulsion silica nanoparticles.<sup>5</sup>

Stöber is well-known procedure which based on hydrolysis and condensation reaction of silicon alkoxides. This method allows the ability to incorporate variety of dye molecules into silica nanoparticles. In addition, it is known from the literature that surface coated silica nanoparticles can be accomplished by using Stöber method. The

modification of synthesized nanoparticles gives them the new abilities. Such nanoparticles which have more useful behavior to clarify the biological assays.

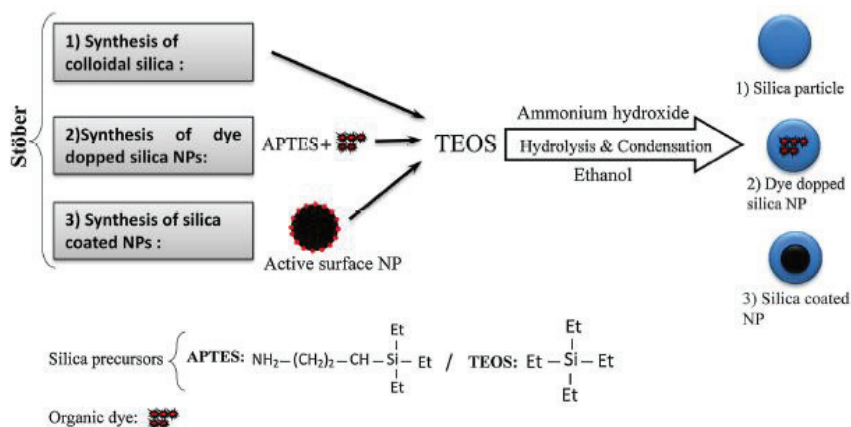


Figure 1.4. Mechanism of Stöber silica nanoparticles.<sup>5</sup>

## 1.2. Synthesis Methods

There are mainly two principal approaches for creating silica nanoparticles, Stöber and Microemulsion methods. However, many methods are generally derived from the Stöber approach. The most important advantages of this method are the synthesis can be scaled up easily, generate monodispersed nanoparticles and time saving. In this thesis, Stöber method was applied to obtain silica nanoparticles.

### 1.2.1. Stöber Method

The Stöber method is basically a type of technique for producing silica nanoparticles, developed in 1968, consists of hydrolysis and condensation reactions of metal alkoxides in a mixture of alcohol and ammonia.<sup>6</sup>

The three main reaction steps occurring in the Stöber process of alkoxysilanes. The schematic representation of the reaction is shown in Figure 1.5. It starts with metal alkoxides  $[\text{M}(\text{OR})_n]$ , such as tetramethoxysilane (TMOS) and tetraethoxysilane (TEOS). The hydrolysis of alkoxy groups (Si-OR) lead to condensation reactions involving silanol groups (Si-OH). Forming of silanol groups can be described as ( $\text{S}_n2$ -

type) reaction. Under alkaline condition of reaction, there is a nucleophilic attack of hydroxide ion at silicon atom with the leaving group which is alkoxy group. Altogether, this process follows condense to Si-O-Si bonds by solvents whether alcohol or water. As the metal alkoxides are generally immiscible in the water, alcohol that has a low molecular weight can be added as a homogenizing agent. During hydrolysis process alcohol is generated as a by-product, that means the addition of alcohol is not always necessary. The reaction rates of hydrolysis and condensation depends on conditions. Under base catalyzed condition, electron withdrawing substituents (-OH and -OSi) cause increase the reaction of rates for hydrolysis and condensation process. Furthermore, alkyl substituents affect the rate of hydrolysis and condensation reaction. The reactivity of alkoxy silanes reduce with the increasing of substituents. Then, TMOS hydrolyzes faster than TEOS.<sup>7</sup> When catalysts are used reactions usually become more rapid. Thus, it is possible to modify the properties of nanomaterials with the help of controlling factors such as reagent concentrations, catalyst and pH.<sup>8</sup>

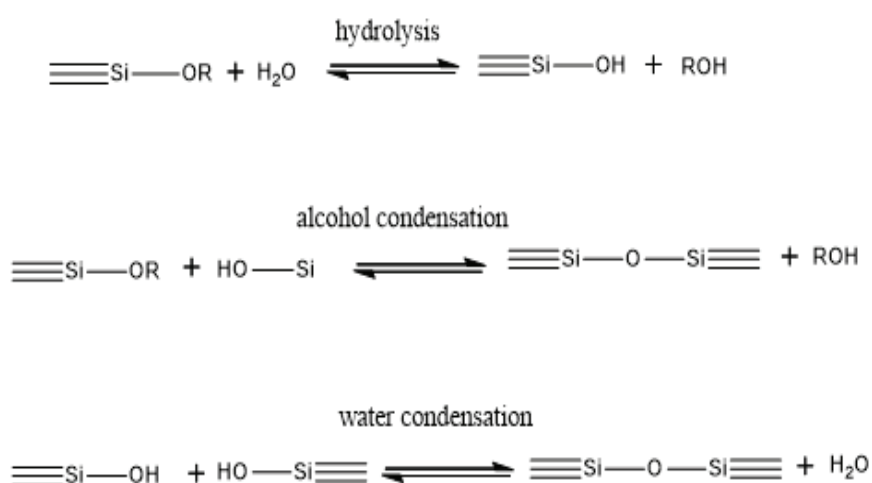


Figure 1.5. Hydrolysis and condensation reactions of TEOS.

To synthesize monodispersed silica nanoparticles which their particle size between 20 and 500 nm, they applied Stöber technique.<sup>9</sup>

In the case of Stöber method, the most common parameters which are morphology and particle size strongly related to amounts of chemicals. One of the study



indicated that modifying the ratio of solvent/metal alkoxide allows to control particle size.<sup>10</sup>

Particle size of synthesized silica nanoparticles were directly proportional to the amount of ammonia by using modified Stöber method.<sup>11</sup>

Qi et al. (2015) prepared monodispersed SiO<sub>2</sub> nanoparticles with the size ranging from 20 to 100 nm. Their synthesis was carried out on the effect of temperature (°C), water and ammonia concentration (mol/L) on both size and the morphology of SiO<sub>2</sub> nanoparticles.<sup>12</sup>

### 1.2.1.1. Effects of Fluorophores

Currently, silica nanoparticles (SiO<sub>2</sub>) doped with fluorescent dyes have been investigated in biological fields. Quantum dots, biological and organic dyes are the example of fluorescent dyes or fluorophores. Adolf von Baeyer contributed to chemistry with his work in organic dyes, and later received the Nobel Prize in Chemistry (1905).

When the electrons reach to ground state again, they emit light of a longer wavelength, which is seen as fluorescence (Figure 1.6).<sup>13</sup>

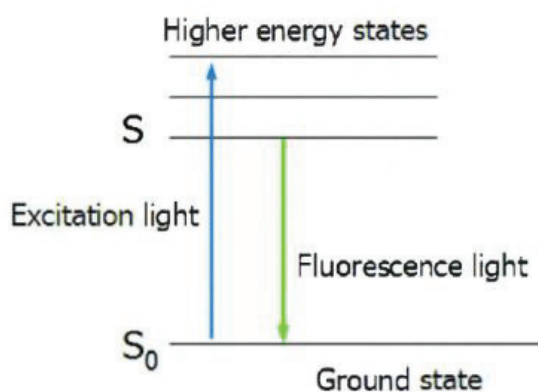


Figure 1.6. Jablonski diagram process within fluorophore.<sup>13</sup>

According to Jablonski diagram, the light is absorbed by the fluorescent dyes, exciting the electrons from their ground state to an excited state which is higher energy level.

From the viewpoint of biomedical applications, dyes should have such as high photostability, quantum yield and absorption at longer wavelengths. Organic types of fluorescent dye such as tetramethylrhodamine isothiocyanate (TRITC) or fluorescein isothiocyanate (FITC) improve the brightness and photostability of particles.<sup>14</sup> The procedure that is to prepare fluorescent silica nanoparticles start when the dye is bound to amine-containing silane agent (for example, 3-aminopropyltriethoxysilane, APTES) by using Stöber method. After that, it will continue with the hydrolyzation and condensation of silicon alkoxide in a mixture of ammonia and alcohol resulting in fluorescent silica nanoparticles.

Organic fluorescent dyes were covalently loaded into silica nanoparticles with the help of Stöber process for the first time.<sup>15</sup>

Wiesner research group yielded fluorescent silica nanoparticles which called Cornell-dots (C-dots). Cyanine which is near-infrared dye was used to label molecules for biomedical purposes. The study was received FDA approval for stage 1 human clinical trial.<sup>16</sup>

In 2015, Grimm et al. reported the properties of fluorophores as concerns specific labeling behavior in bio-applications. They altered the structure of tetramethylrhodamine by replacing N,N-dimethylamino and azetidine rings so that enhance the photostability and brightness of dye molecule.<sup>17</sup>

#### **1.2.1.2. Effects of Surface Functionalization**

The application of surface functionalization affects the particle size, charge, hydrophobicity, hydrophilicity and surface chemistry of nanoparticles. Surface functionalization is an effective and often simpler way of altering the surface properties of a material to achieve specific aims such as inducing a desired bio-response. Different approaches include silane-coupling agents, physical adsorption and layer-by-layer assembly have been developed based on the surface affinity properties of nanoparticles. Altering the surface chemistry which helps to enhance biocompatibility and biodistribution of nanoparticles.<sup>18</sup> Thus, modifying the nanoparticles are the key factor in nanoparticles-cellular interactions.

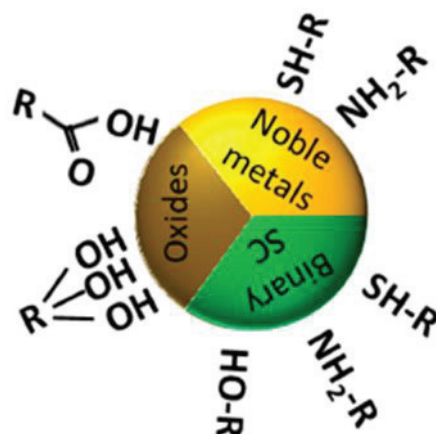


Figure 1.7. Commonly used functional groups binding different nanoparticles.<sup>19</sup>

Noble metals, oxides and binary semiconductor (SC) types of nanoparticles could be functionalized with some functional groups that were given in Figure 1.7.<sup>19</sup> For example, SC nanoparticles can be coated with the thiols (R-SH), hydroxyl (R-OH) and amino groups (R-NH<sub>2</sub>). The example of some semiconductor nanoparticles are Si, SiC, ZnSe, CdS.

Generalova et al. synthesized photoluminescent types of nanomaterials which called Lanthanide-doped upconversion (UCNPs). Tetramethylammonium hydroxide (TMAH) was used to transfer the synthesis organic to aqueous phase. TMAH encapsulated nanoparticles that exhibited bright PL NPs. Therefore, they demonstrated the biomedical application of TMAH-modified NPs.<sup>20</sup>

Gomes and co-workers have developed modifications of fluorescent silica nanoparticles to increase colloidal stability for bioimaging purposes. 3-aminopropyltriethoxysilane (APS) and polyethylene glycol (PEG) were introduced to fluorescent SiNPs to improve biological response. PEG was a good choice for the surface modification due to its low-toxicity.<sup>21</sup>

Non-functionalized silica nanoparticles have negatively charged because of the ionization of hydroxyl groups. However, changing surface chemistry of nanoparticles cause the different zeta potential value from the bare SiNPs. Silica nanoparticles were made positively charged after modified with PEG QA(quaternary amine). The results were shown that the excretion which means eliminates the metabolic waste was greater when the SiNPs functionalized with PEG-QA group.<sup>22</sup>

Positively charged nanospheres were found internalization into the cell differ from the other charged particles. Nanosphere which have +20mV zeta potential were most suitable one, because it internalized to cell easily.<sup>23</sup>

### 1.3. Cell-based Assays

#### 1.3.1. Bioimaging

As mentioned above, dye-doped and surface modification ability of silica nanoparticles have extent of improvement in bioimaging areas. It should be emphasized that wavelength, brightness, photostability and biostability are the important characteristics of the dyes to be successful bioprobes.<sup>24</sup> Generally, conventional dyes are photobleached easily and that means their staining sensitivity can be reduced. However, fluorescent nanoparticles have many benefits over the conventional organic dye for bioimaging application.<sup>25</sup> Fluorescein dye is one of the FDA approved fluorophores for biomedical areas.

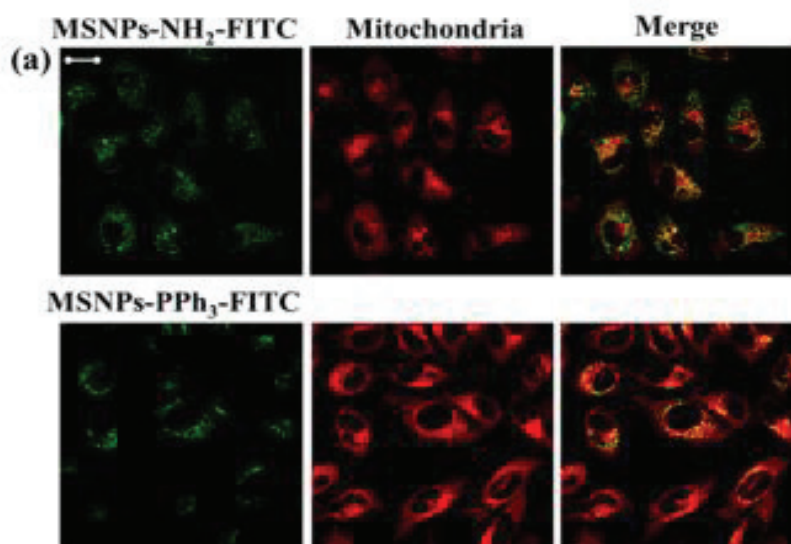


Figure 1.8. (Cont. on next page)

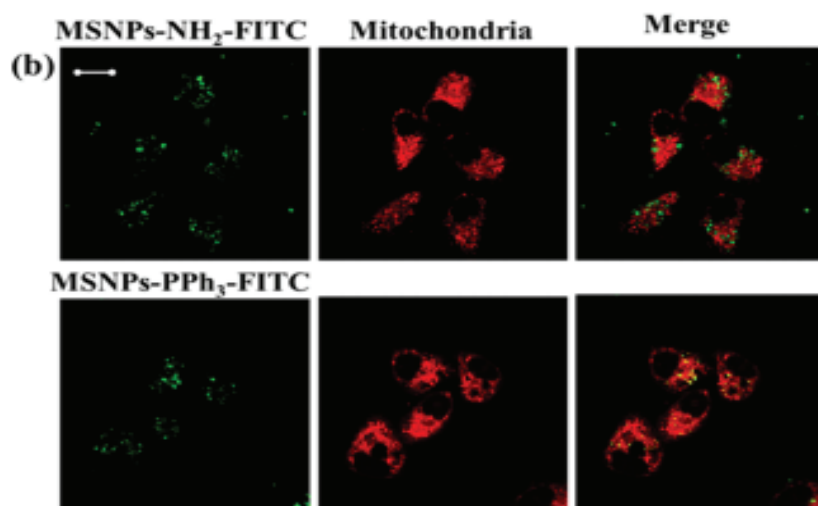


Figure 1.8. Confocal laser scanning microscope images of (a) HeLa cells and (b) HepG2 cell lines with MSNP both coated with  $\text{NH}_2$  and  $\text{PPh}_3$ .<sup>27</sup> (Cont.)

Furthermore, surface of dye-doped silica nanoparticles are suitable to coating with functional groups. Using dye and surface modification process can be used to enhance both aqueous dispersibility and bioconjugation capability. These strategies provide the effective detection in cells.

Another important point in bioimaging is that cell staining. It is a method that can be commonly used to better visualize cells under a microscope. There are several examples of probes such as carmine, DAPI, methylene blue, rhodamine, TMRE, JC-1 and Mito-Red. Each of them are applied to stain different organelles. Mito-red, TMRE and JC-1 which are types of probes are convenient to label mitochondria.<sup>26</sup>

HeLa cells and HepG2 cells were treated with MSNP- $\text{NH}_2$ -FITC ( $50\mu\text{g/ml}$ ) and MSNP- $\text{PPh}_3$ -FITC ( $50\mu\text{g/ml}$ ) and the cell images were obtained by using confocal microscopy. The surface functionalization of MSNPs to be target in mitochondria organelle were demonstrated. Mitochondria is critical organelle in terms of ATP production and pathway of cell death. For that purpose, they functionalized nanoparticles surface with both  $\text{NH}_2$  and  $\text{PPh}_3$  groups. As seen from the Figure 1.8. mitochondria was stained with the Mito-Tracker-Red. FITC labeled MSNPs were indicated as green dots. Considering both nanoparticles and cell lines,  $\text{PPh}_3$  modified silica nanoparticles show better overlapping (yellow color) than MSNP- $\text{NH}_2$ -FITC.<sup>27</sup>

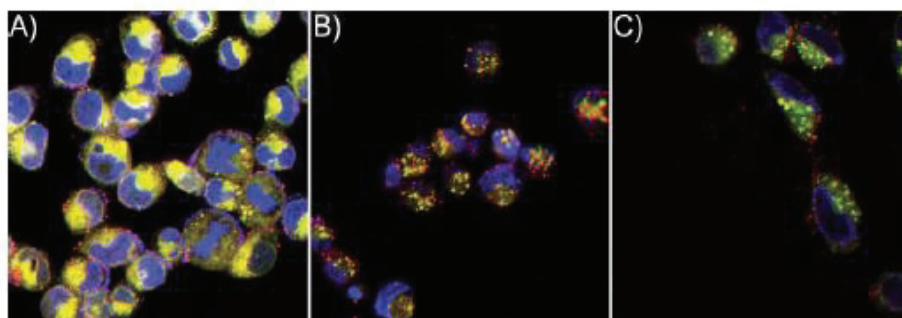


Figure 1.9. Confocal microscope images of MDA-MB-468 cell lines and mesoporous silica NPs with different sizes. (A) 190 nm, (B), 420 nm and (C) 1220 nm.<sup>28</sup>

In Figure 1.9., SiNPs were labeled with Rhodamine B which gave the red signal. Moreover, blue and green dots represents the nuclei and lysosomes, respectively. LysoTracker Green DND-26 and Hoechst 33258 were applied to labeling lysosomes and nuclei of MDA-MB-468 cell lines. They found that the smallest MSNPs were more localized into the lysosomes and cells.<sup>28</sup>

### 1.3.2. Toxicology

Nanotoxicology is the developing area that deals with the toxicological profiles of nanoparticles. Toxicity of nanoparticles should be considered in biological studies. SiNPs become promising candidate due to their stability, safety, biocompatibility properties. In fact, SiNPs have been used as biomaterials for a long time.<sup>29</sup> Biocompatibility is the required behavior of nanomaterials in order to be chosen in biological nanosystems.<sup>30</sup> It means that there should not be observed any toxic effects when the nanoparticle and cell interact with each other.

Studies have shown that physicochemical properties like size, shape, charge, surface coating are collectively influence toxicity of silica nanoparticles behavior. Besides, toxicology of nanoparticle also depends on the types of cell lines and incubation time.<sup>31</sup>

According to literature studies, toxicological profile of silica nanoparticles are depends on some parameters such as cell line, concentration, particle size and time. (Table 1.1.)

Table 1.1. Toxicity of SiNPs according to literature studies.

Cell Line	Types of SiNPs	Amount ( $\mu\text{g/ml}$ )	Size (nm)	Time (hours)	Viability (percent)	References
A549	FITC-SiNPs	15	15	24	50	Hsiao et al. (2014)
A549	FITC-SiNPs	50	60	24	50	
THP-1 macrophage	FITC-SiNPs	10	15	24	50	
THP-1 macrophage	FITC-SiNPs	18	60	24	50	
A549	NH <sub>2</sub> -SiNPs	<250	22.7	72	98	Nowak et al. (2014)
A549	COOH-SiNPs	<250	23.2	72	97	
HCECs	SiNPs	100	50	24	90	Kim et al. (2017)
HCECs	SiNPs	100	100	24	70	
HCECs	SiNPs	100	150	24	75	
HCECs	SiNPs	100	50	48	90	
HCECs	SiNPs	100	100	48	90	
HCECs	SiNPs	100	150	48	90	
HeLa	FSNP-SD	100	100	48	80.85	Xia et al. (2013)
3T3	FSNP-SD	100	100	48	80.9	
A549	Crystalline SiNPs	10	15	24	98	Lin et al. (2006)
A549	Crystalline SiNPs	100	15	24	83.4	
A549	Crystalline SiNPs	10	15	48	91.9	
A549	Crystalline SiNPs	100	15	48	68.1	
A549	Crystalline SiNPs	10	15	72	82.8	
A549	Crystalline SiNPs	100	15	72	54.6	
MC3T3-E1	FITC-labeled SNs	20	121	24	97	Xu et al. (2014)
MC3T3-E1	FITC-labeled SNs	20	310	24	96	
MC3T3-E1	FITC-labeled SNs	20	646	24	100	
MC3T3-E1	FITC-labeled SNs	100	121	24	82	
MC3T3-E1	FITC-labeled SNs	100	310	24	80	
MC3T3-E1	FITC-labeled SNs	100	646	24	81	

WST-1, XTT and MTT are the types of viability assay for routine applications in cell biology. Cells (A549 and THP-1 macrophage) were exposed to SiNPs according to WST-1 assay to evaluate toxicity of NPs. A549 had an IC<sub>50</sub> value of 15 and 50 $\mu\text{g/ml}$  for 15 nm and 60 nm particle size at 24h. In the case of THP-1 macrophage had an IC<sub>50</sub> (50% cell viability) value of 10 and 18 $\mu\text{g/ml}$  for the 15 nm and 60 nm at 24h. The result demonstrates that toxicity of 15nm and 60nm SiNPs were dose-dependent. Additionally, toxicity of synthesized silica nanoparticles was also dependent on the cell line.<sup>32</sup>

Cytotoxic effects of SiNPs were investigated for lung epithelial cells (A549) with the help of MTT assay. No significant toxic effect was detected below 250 $\mu\text{g/ml}$  for both -NH<sub>2</sub> and -COOH functionalized particles at 72h.<sup>33</sup>

Kim et al. reported safety of 50 nm, 100 nm and 150 nm sized SiNPs which was nonporous by utilizing the primary culture of human corneal epithelium (HCECs). At 24h, 50 nm and 100 nm sized particles were showing a small decrease in cell viability as 70%. There was not observed any toxic effect of three NPs to HCECs for

100 $\mu$ g/ml at 48h. Therefore, their study proved the nontoxicity of 50 nm, 100 nm and 150 nm sized SiNPs in HCECs.<sup>34</sup>

Toxicity of types of fluorescent silica nanoparticles were explored by using Hela cells and 3T3 cells. The result showed that the viability of particles which have 100nm size were approximately 80% for both cells lines at 48h.<sup>35</sup>

In another toxicology study, they indicated that SiO<sub>2</sub> NPs 15 nm in size were time and dose dependent cytotoxicity.<sup>36</sup>

Xu et al. (2014) selected the MC3T3-E1 to measure toxicity of engineered silica nanoparticles which have 121 nm, 310 nm and 646 nm in size for 20 $\mu$ g/ml and 100 $\mu$ g/ml. For this purpose, FITC-labeled SNs were exposed to cell and evaluated percentage of viability by using MTT assay. They suggested that toxicity of FITC-labeled SNs was dose-dependent.<sup>37</sup>

#### **1.4. Purpose of This Study**

The purpose of the study is to change behavior of silica nanoparticles by whether using dye or functionalize the surface with the help of modified Stöber technique. Additionally, surface functionalized dye-doped SiNPs is helping understand the particle-cell interactions.



## CHAPTER 2

### SYNTHESIS AND SURFACE FUNCTIONALIZATION OF FLUORESCENT SILICA NANOPARTICLES

#### 2.1. Introduction

In this chapter, (-) potential silica nanoparticles and (+) potential silica nanoparticles will be discussed. Negative potential silica nanoparticles and positive potential silica nanoparticles were produced from the modified Stöber method. Stöber et al. (1968) introduced the process based on hydrolysis and condensation of tetraethyl orthosilicate (TEOS) to obtain monodisperse silica nanoparticles.<sup>6</sup> Fundamentally, silicates or silicon alkoxides are added in a mixture of water/alcohol and ammonia as a catalyst. Metal alkoxides  $M(OR)_n$  are great single source molecular precursor for oxide synthesis because of their high reactivity and structure properties.

Fluorescent SiNPs is the type of silica nanoparticle that incorporate of dye into the particle have been used for bioanalytical purposes. When dye-doped NP probes are used, a biomolecule recognition event signaled by one NP will link thousand of dye molecules to one target molecule, thus greatly enhance the fluorescence signal.

To facilitate the coupling of particles for specific targets in cell, surface modification of fluorescent SiNPs have been developed. Surface modification can dramatically change the properties of silica NPs hence the performance of them in biomedical applications depending on which coating material are linked on the surface.

Fluorescent loaded silica nanoparticles have important role with the attractive features such as photostability, brightness which provide sensitive imaging of cells.<sup>38</sup> Fluorescein isothiocyanate (FITC) is a type of organic dyes of fluorophores which has excitation and emission spectrum peak approximately 495nm/519nm. Thus, the derivative of fluorescein or FITC absorbs the blue light, resulting fluorescence occurs at the yellow-green wavelengths.<sup>39</sup>

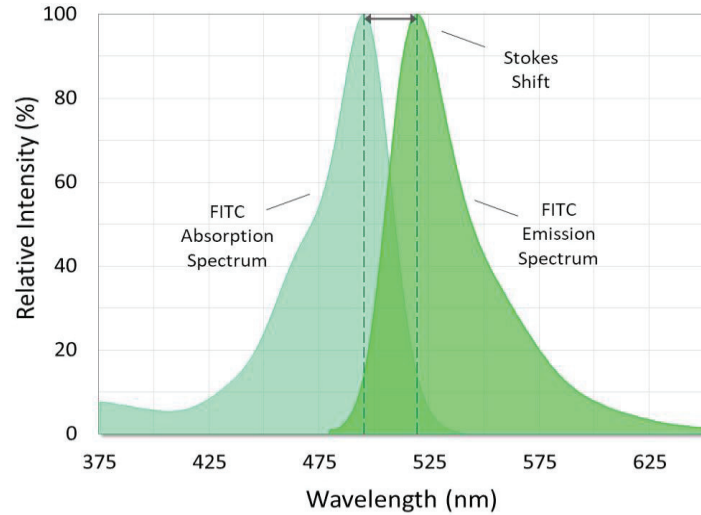


Figure 2.1. Absorption and fluorescence spectrum of FITC.<sup>40</sup>

As can be seen in Figure 2.1.,<sup>40</sup> the difference between the excitation maxima and the emission maxima of fluorophore is called its Stokes shift. To prevent undesired background interference, large Stokes shift ( $\Delta\lambda > 80\text{nm}$ ) have been evolved, but not clarified clearly. The extent in the excitation and emission spectra of fluorescent dyes means, it does not absorb the photon that is self-emitted. For this reason, fluorophores helping to label specific parts of biological samples.<sup>41</sup> FITC with an isothiocyanate group makes it reactive towards amine and sulfhydryl groups which usually found in biomolecules.

The preparation of the positively potential SiNPs was depend on N-((trimethoxysilyl)propyl)-N,N,N-trimethylammonium chloride (TMAC) which can classified in the quaternary ammonium salts. To investigate the surface interaction of particles with cell, TMAC-silane was used. They have particularly contain 12-18 carbon atoms chains and a nitrogen atom that is thus positively charged.<sup>42</sup>

After the synthesis process, characterization techniques should be involved to obtain information of particles such as size, charge and surface chemistry. There are instruments for characterization like dynamic light scattering (DLS), spectrofluorometer (PL), fourier-transform infrared spectroscopy (FTIR), scanning electron microscopy (SEM), scanning transmission electron microscope (STEM) and inductively coupled plasma atomic emission spectroscopy (ICP-OES).

Dynamic light scattering (DLS) is dependent on Brownian motion of particles suspended within liquid. Brownian motion is related to particle movement that means

smaller particles are moving at higher speeds than larger particles. The relation between the speed and size can be measured by using Stokes-Einstein equation. The following equation includes hydrodynamic diameter ( $dH$ ), Boltzmann constant  $k$  ( $m^2 \text{ kgs}^{-2} \text{ K}^{-1}$ ), temperature  $T$  (Kelvin), solvent viscosity  $\eta$  (Pa.s) and diffusion coefficient  $D$  ( $m^2/s$ ).

$$dH = \frac{kT}{3\pi\eta D} \quad (1.1)$$

The calculated particle diameter in dynamic light scattering is called the hydrodynamic diameter. Hydrodynamic diameter means hydration layer which surrounding the particle or molecules.<sup>43</sup>

Spectrofluorometer is an analytical device related to fluorescence which is short-lived classified into photoluminescence spectroscopy. It is continue gaining huge interest in science for quantitative analysis of samples. Spectrofluorometer gives us spectrum that is function of wavelength. Light source is located in a 90 degree angle since reduce scatter light and increase sensitivity. Emission of electromagnetic radiation takes place visible light, resulted in excitation of molecules.

All spectroscopy methods based on electromagnetic radiation. It can be characterized by its wavelength  $\lambda$  ( $\mu\text{m}$ ) frequency  $\nu$  (Hz) and energy  $E$  (J). There are related to each other as seen from the following equation, where  $c$  is for speed of light ( $3.00 \times 10^8 \text{ ms}^{-1}$ ) and  $h$  is Plank's constant ( $6.63 \times 10^{-34} \text{ Js}$ ).

$$\lambda\nu = c \quad (1.2)$$

$$E = \frac{hc}{\lambda} \quad (1.3)$$

Ultraviolet radiation, visible light and infrared radiation corresponding to wavelengths of less than 400 nm, between 400 and 700 nm, longer than 700 nm, respectively. Figure 2.2., indicates the schematic representation of electromagnetic radiation.<sup>44</sup>

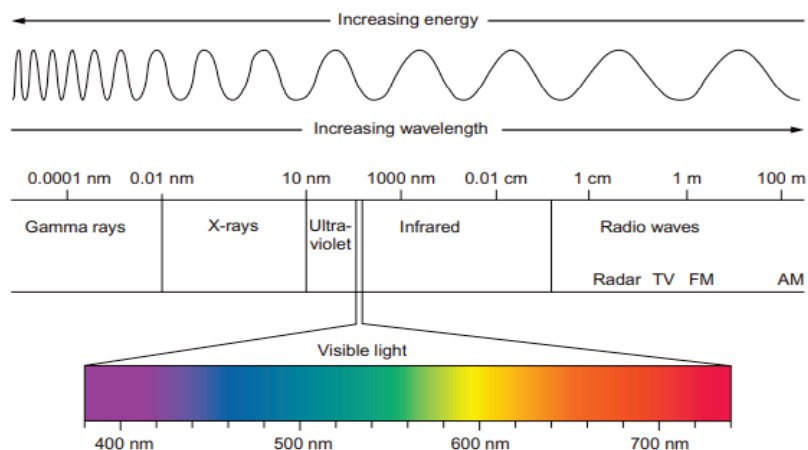


Figure 2.2. Electromagnetic spectrum.<sup>44</sup>

Fourier transform infrared spectroscopy (FTIR) techniques is used to recognize characteristic functional groups present in a sample.<sup>45</sup> FTIR gives the infrared spectrum which x axis corresponds to wavenumber ( $\text{cm}^{-1}$ ) and y axis corresponds to %Transmittance. Wavenumber is equal to reciprocal of the wavelength ( $1/\text{wavelength}$ ). FTIR functional groups table were given. (Table 2.1.)

Table 2.1. Infrared spectra of some common functional groups.

frequency in $\text{cm}^{-1}$	bond	functional group
3640-3610 (sharp)	O-H stretch	alcohols
3500-3200 (broad)	O-H stretch	alcohols
3400-3250 (medium)	N-H stretch	1° 2° amines, amides
3300-2500	O-H stretch	carboxylic acid
3100-3000	C-H stretch	aromatics, alkenes
3000-2850	C-H stretch	alkanes
3000-2800 (strong)	N-H stretch	amine salt
2260-2210	C=N stretch	nitriles
2150-2000	Si-H	amorphous silicon
1760-1665	C=O stretch	carbonyls
1760-1690	C=O stretch	carboxylic acid
1650-1580	N-H bend	1° amines
1600-1585	C-C stretch (in ring)	aromatics
1470-1450	C-H bend	alkanes
1360-1290	N-O symmetric stretch	nitro compounds
1335-1250	C-N stretch	aromatic amines
1230-940	Si-O	silicon monoxide
1130-1000	Si-O-Si	siloxanes
950-810	Si-OH	silanol

Electron microscopes has advantages over the traditional light microscopes in terms of resolution and magnification.<sup>46</sup> Scanning electron microscope (SEM) and scanning transmission electron microscope (STEM) are the example of electron microscopes. SEM is a powerful method that use the electron to utilize the three dimensional image of the specimen. It mainly consist of electron gun, condenser lenses, objective aperture, scan coils, chamber, detector. Secondary electron detector is used to obtain information about topographic image. Backscatter electron detector is useful for illustrating contrast in composition. When scanning electron microscope equipped with the energy dispersive X-ray detector (EDS or EDX) it is possible to acquire chemical composition of sample. STEM combines both the scanning electron microscope and tranmission electron microscope. The STEM technique has two observation modes which is bright-field and dark-field mode. Detection of both modes were developed by Crawford and Liley at first.<sup>47</sup> In bright-field image, particles seem as dark because the incident electrons are scattered at high angles. In dark-field image, particles appear bright.

ICP-OES is a elemental analysis for determination of elements in different samples. Due to it has high temperature, excitation, vaporization, atomization and ionization process can be achieved successfully for comprehensive elements in a various samples. It has the potential to measure concentration of elements while light emitting at specific wavelength.<sup>48</sup>

## **2.2. Experimental**

### **2.2.1. Chemicals and Reagents**

Tetraethyl Orthosilicate (TEOS 98%, Aldrich), ammonium hydroxide (NH<sub>4</sub>OH 28-30%, Aldrich), absolute ethanol (99.9%, Merck), fluorescein isothiocyanate (FITC, isomer I, Aldrich), 3-Aminopropyl triethoxysilane (APTES, 99% ,Alfa Aesar) and N-((trimethoxysilyl)propyl)-N,N,N-trimethylammonium chloride (TMAC, 50% in methanol, Alfa Aesar) were used throughout the study in order to prepare both (-) potential and (+) potential SiNPs.

### 2.2.2. Instrumentation

DLS (Malvern Zetasizer Nanoseries-NanoZS, Dynamic Light Scattering), also known as photon correlation spectroscopy, was used to determine the particle sizes and the zeta potentials of silica nanoparticles.

Absorption and fluorescence spectra were recorded by PL (FS5 Edinburgh Spectrofluorometer, Photoluminescence).

FTIR (Perkin Elmer UATR-TWO, Fourier-Transform Infrared Spectroscopy) was used to analyze molecular functional groups in particles.

SEM (Philips XL-30S FEG, Scanning Electron Microscopy) and EDS (Energy Dispersive Spectroscopy) were applied to investigate the morphologies and elemental compositions of synthesized SiNPs, respectively.

SEM (FEI QUANTA 250 FEG, Scanning Electron Microscopy) with STEM (Scanning Transmission Electron Microscope) detector were used to characterize the nanoscale of specimen.

ICP-OES (Agilent 7500ce Octopole Reaction System) was used to quantify the elemental concentration with the sample.

### 2.2.3. Synthesis of (-) Potential SiNPs

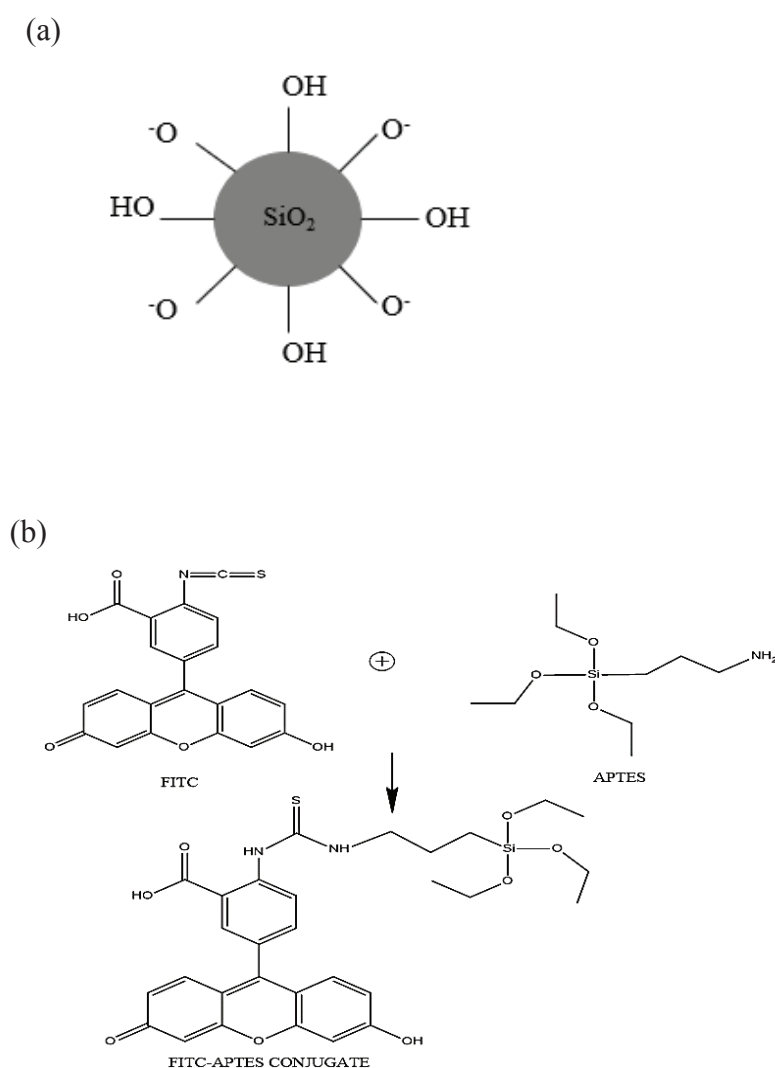
Silica nanoparticles were synthesized using well-known Stöber process. It includes hydrolysis and condensation of tetraethyl orthosilicate as a silica source, ammonia solution as a catalyst in the presence of ethanol solvent. The reagents that were used in the synthesis of silica nanoparticles have already been optimized in our laboratory.<sup>11</sup>

To demonstrate bioimaging applications, modified Stöber method was applied for the preparation of (-) SiNPs with the help of FITC and APTES molecules.

In the first step, fluorescent dye was prepared. The molar ratio between FITC and APTES was adjusted 1:1.<sup>49</sup> Briefly, FITC ( $6.42 \times 10^{-6}$  mmol) was weighed as 2.5 mg. APTES ( $6.42 \times 10^{-6}$  mmol) and absolute ethanol (1ml) were prepared as a stock solution. From that solution, 150  $\mu$ l was added to FITC producing a fluorescent conjugate. It must be very careful while using APTES for preparation of dye process. It can react with the moisture in the air and this cause aggregation in SiNPs. The solution of the APTES-

FITC conjugate was kept in the dark under dry nitrogen atmosphere and stirred for 24h. Protection from the light of the dye conjugate is necessary in order to prevent photobleaching. APTES-FITC conjugate leading to the formation of thiourea linkage due to specific binding of amine group of APTES and cyanate group of dye.<sup>50</sup>

In Figure 2.3., (a) schematic representation of bare silica nanoparticles were given. Surface charge of untreated SiNPs were found highly negative, because it was made up of the hydroxyl and oxygen groups. Figure 2.3., (b) illustrates the structures of APTES-FITC conjugate.



In the second step, (-) silica nanoparticles were prepared. Ethanol (30ml), dye conjugate (0.1ml), ammonia solution (0.2ml), and tetraethyl orthosilicate (1.2ml) were added under N<sub>2</sub> and stirred for 24 hours. Figure 2.4. indicates the steps of experiment for (-) silica NPs.

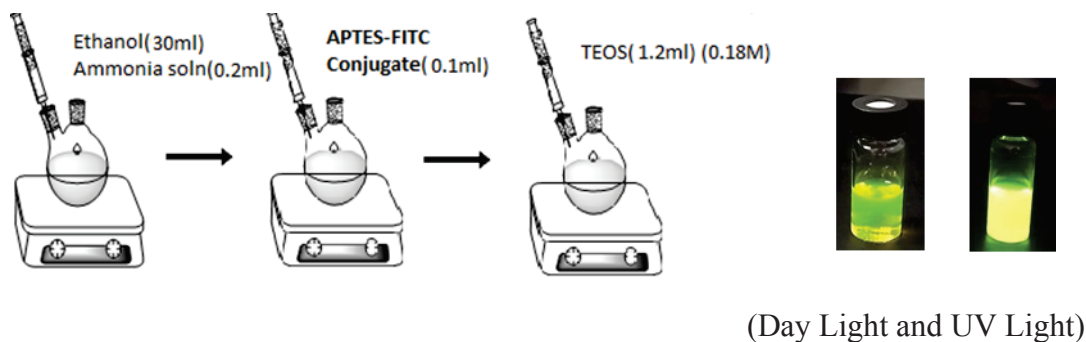


Figure 2.4. Preparation procedure of (-) potential silica nanoparticles.

#### 2.2.4. Synthesis of (+) Potential SiNPs

Silica nanoparticles have been studied widely due to their favorable surface chemistry. NP-cell interactions strongly depend on the NP physicochemical features. As the biological system will be related to the surface properties of silica nanoparticles, (-) potential SiNPs have functionalized by the quaternary amine functional silanes. The easiest and most used method for functionalization of the nanoparticle surface is the use of silanes as anchor chemistry. For that purposes, TMAC (283 $\mu$ l) and TEOS (116 $\mu$ l) was added into synthesis of (-) potential silica nanoparticles in a N<sub>2</sub> atmosphere and carried out for 1 day. Adding of TEOS was useful to enhance silicates ratio in the particles. The structure of TMAC was given in Figure 2.5. (a). Schematic representation of surface functionalization of (-) SiNPs using TMAC were given in Figure 2.5. (b). The steps of experiment were shown in Figure 2.6. Overall, silica nanoparticles solutions were centrifuged at 17.500 RPM for a 15 minutes to remove unreacted species.



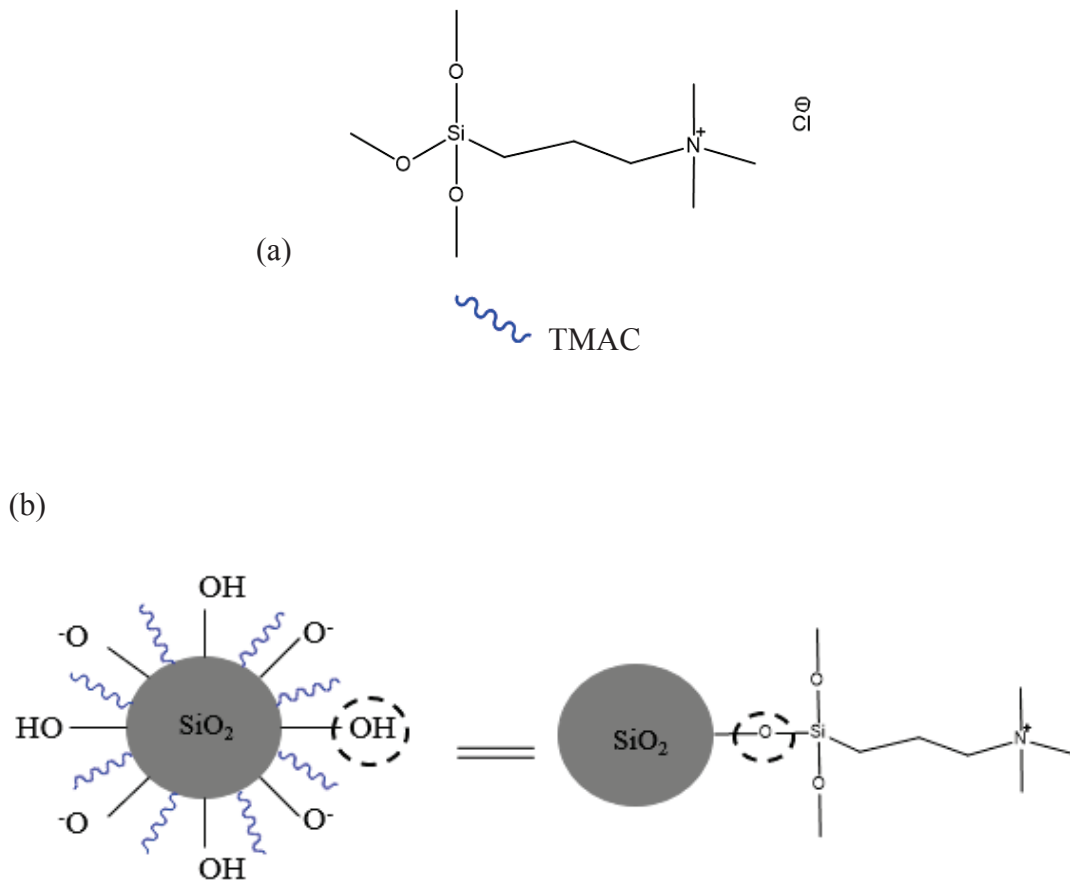


Figure 2.5. Summary of (a) structures of TMAC molecule, (b) schematic representation of (+) potential silica nanoparticles.

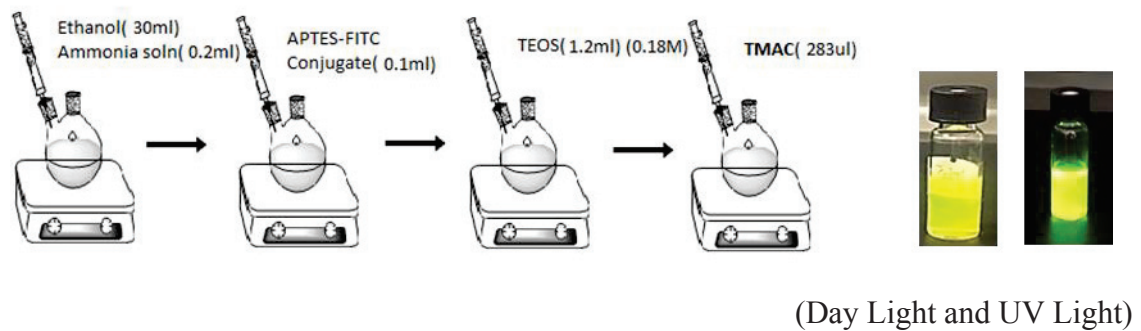


Figure 2.6. Preparation procedure of (+) potential silica nanoparticles.

## 2.3. Results and Discussion

### 2.3.1. Characterization of (-) and (+) SiNPs

Florescent silica nanoparticles and N-((trimethoxysilyl)propyl)-N,N,N-trimethylammonium chloride functionalized silica nanoparticles were obtained by using modified a Stöber method. Dynamic Light Scattering was applied for the characterization of (-) and (+) pot. SiNPs in terms of their sizes and surface charges. Figure 2.7. displays the nanoparticle size of (-) SiNPs(10nm) and (+) SiNPs (20nm). As TMAC was generally used as amination reagent, <sup>51</sup> TMAC-functionalized SiNPs has more amine group than (-) SiNPs in that case, the particle size of (+) silica nanoparticles were obtained larger than 10nm.

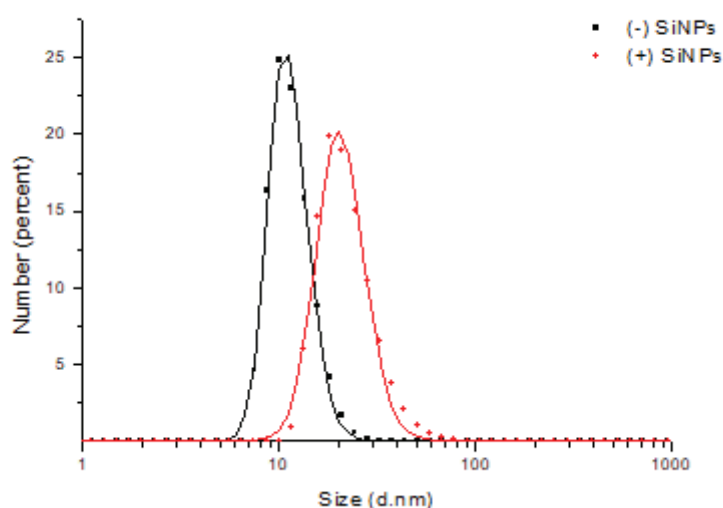


Figure 2.7. The sizes of the (-) SiNPs and (+) SiNPs.

During the zeta potentials measurement, they were repeated for the three times based on DLS principle. The average zeta potentials for both (-) SiNPs and (+) SiNPs were given in Figure 2.8. These values were determined as -15mV and +30mV respectively. Amine group of TMAC makes silica nanoparticles more positive.

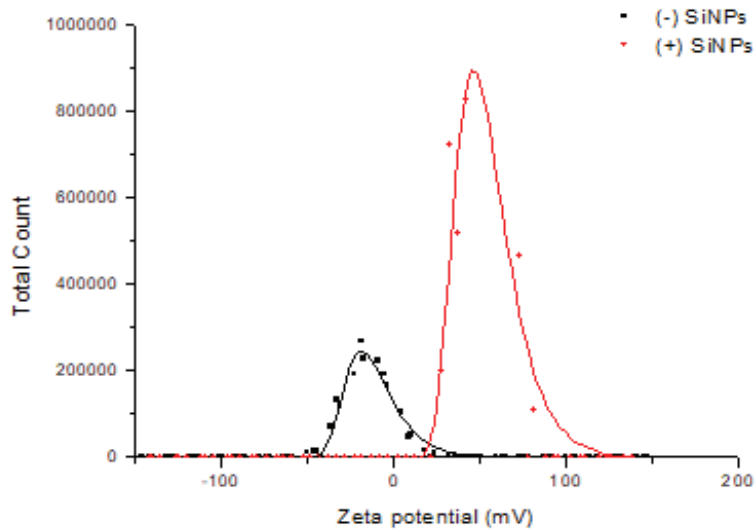


Figure 2.8. The zeta potentials of the (-) SiNPs and (+) SiNPs.

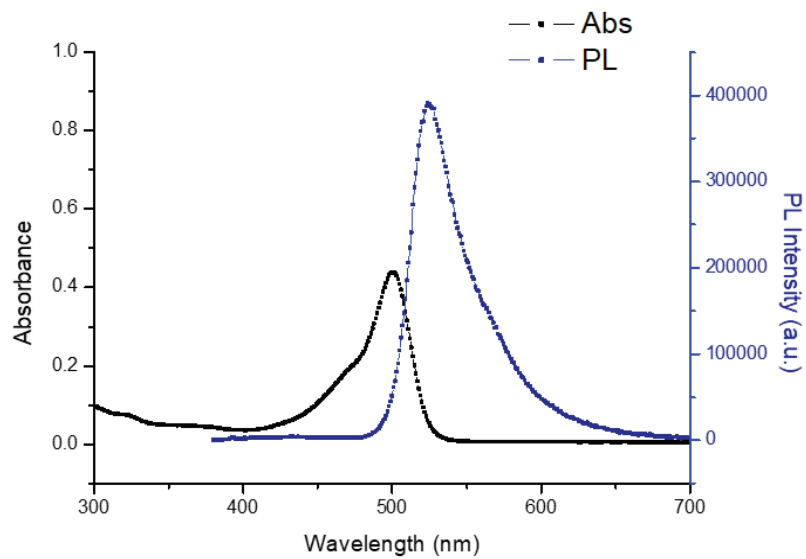


Figure 2.9. The absorption and PL spectra of silica nanoparticles.

The emission and absorption spectra of the silica nanoparticles were recorded by Spectrofluorometer (Figure 2.9.). The absorption and emission maximum of SiNPs was found to be at 495nm, 515nm respectively. Both values were confirmed the FITC dye molecule, it was excited by blue light and emits the green fluorescence.

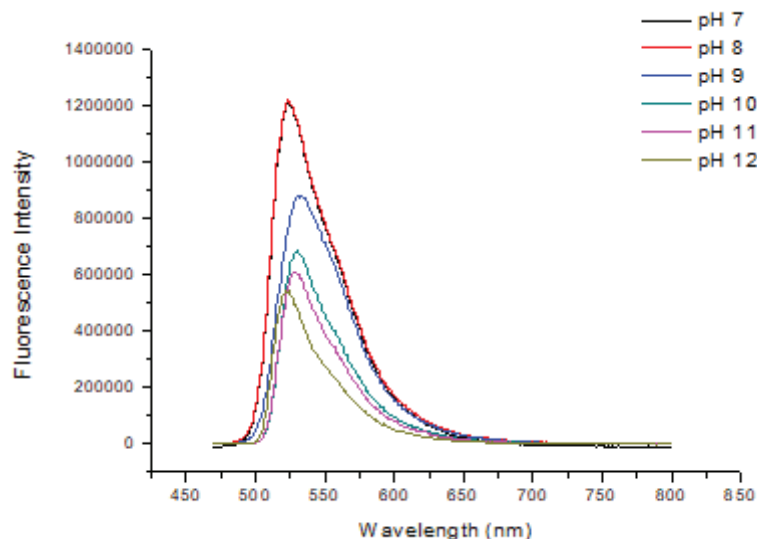


Figure 2.10. The pH dependence of fluorescence intensity of free FITC.

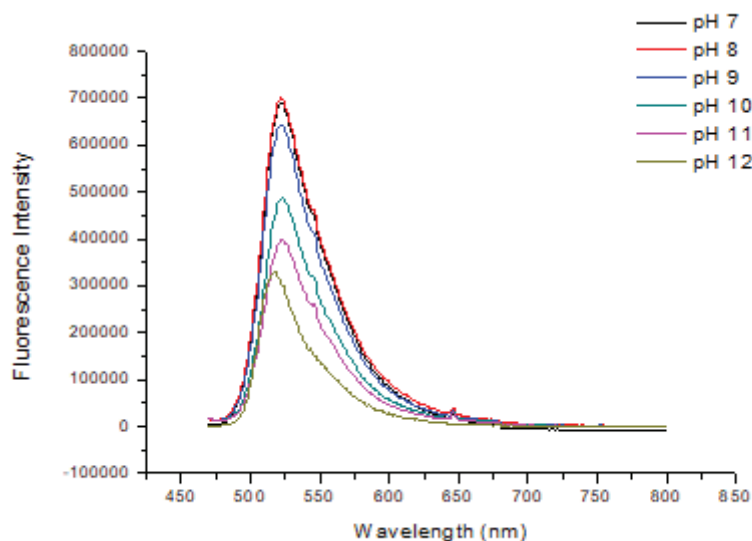


Figure 2.11. The pH dependence of fluorescence intensity of silica nanoparticles.

In order to verify the protection of FITC-dye molecules by the synthesized silica nanoparticles, three factors were investigated such as pH effects, solvents effects and the quench effects. As can be shown in Figures 2.10-11., Fluorescence intensity of silica nanoparticles were less affected than free FITC in terms of pH. The pH of solution (aqueous) was altered from 7 to 12 by using NaCl and HCl. Fluorescence intensity was beginning to be affected at pH=10 for the silica nanoparticles. We have applied pH

value at approximately 9 in our study, so it does not affect the results. Besides, there was not any change of spectral shape observed in the presence of silica nanoparticles until pH 12. However, at pH=9 fluorescence intensity was already decreased concerning the free dye. Additionally, more changes in peak positions were observed for free dye.

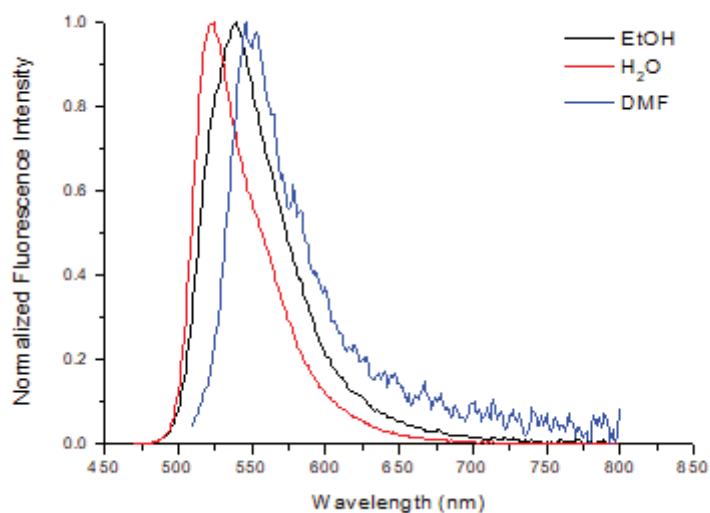


Figure 2.12. Solvent effect: fluorescence intensity of free FITC.

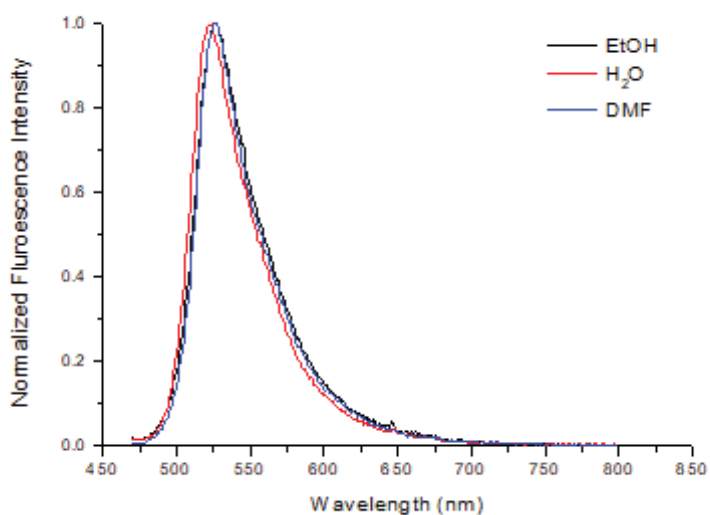


Figure 2.13. Solvent effect: fluorescence intensity of silica nanoparticles.

Another factor was that solvent effects on free-FITC and particles as given Figure 2.12-13. Solvent changes the reactivity of reducing agent and precursors, while either stabilizing the nanoparticles or promoting their aggregation. Here, we tested three solvents such as two polar protic solvents (ethanol, water) and polar aprotic solvent (dimethylformamide). Polar aprotic solvents contain no hydrogen atoms connected to an electronegative atom and they are not capable of hydrogen bonding. Both free-FITC and particles were soluble in all three solvents.

In Figure 2.12, solvatochromatic effect has seen which was about some spectral changes when the substance was miscible in a variety of solvents. This effect resulting in red shift which was termed positive solvatochromism with increasing solvent polarity.<sup>52</sup> Red shift in fluorescence spectrofluorometry corresponds to a spectral shift to higher wavelengths (lower energy). In the matter of particles (Figure 2.13.), there has not any changing of wavelength maximum. Solvents have not reach to the FITC in silica nanoparticles, so effective protection was supplied by the synthesized particles.

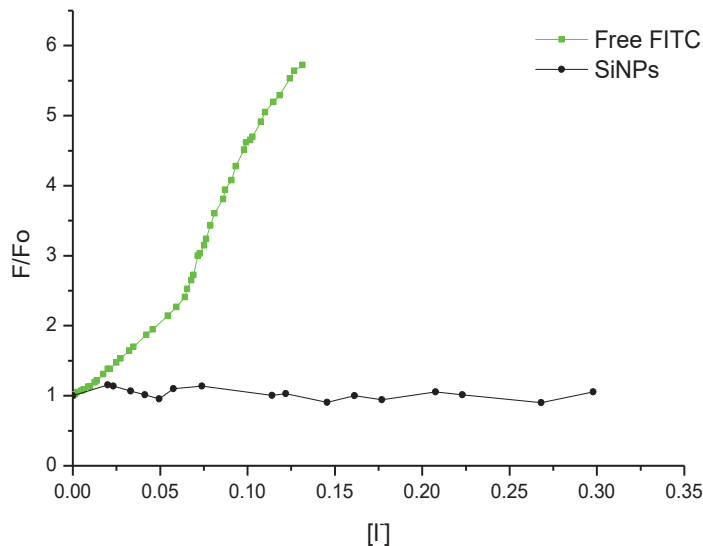


Figure 2.14. Stern-Volmer plot of quenching effect for both free FITC and silica nanoparticles in the presence of quencher I.

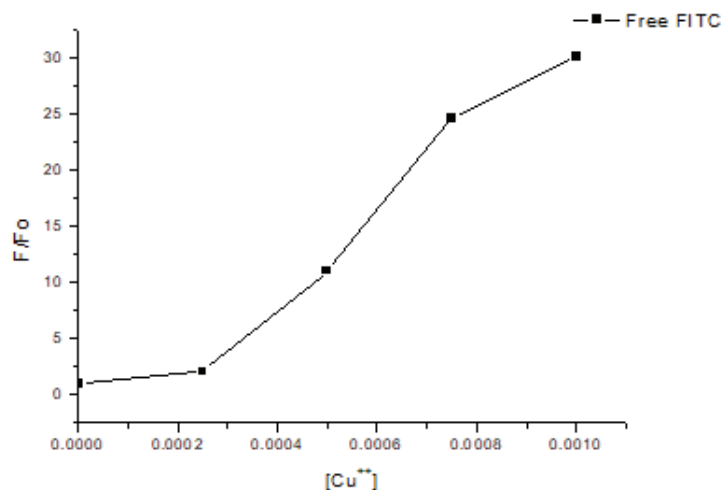


Figure 2.15. Stern-Volmer plot of quenching effect for free FITC in the presence of quencher Cu<sup>2+</sup>.

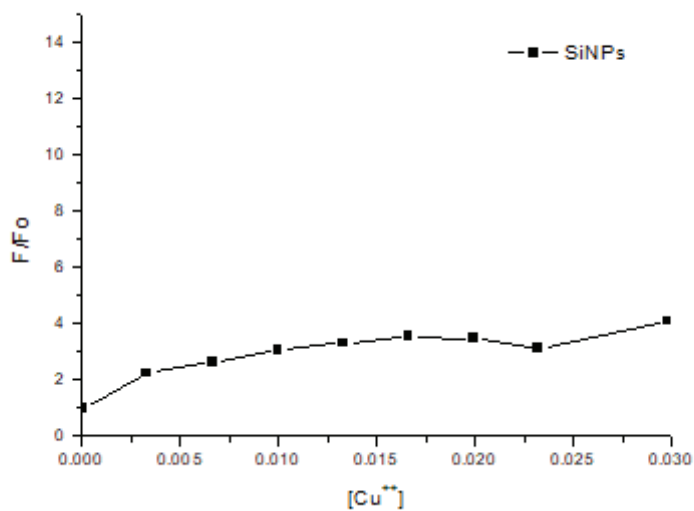


Figure 2.16. Stern-Volmer plot of quenching effect for silica nanoparticles in the presence of quencher Cu<sup>2+</sup>.

Stern-Volmer plot showing reduction in fluorescence intensity or quenching processes for silica nanoparticles (Figure 2.14-15-16.). In the simplest case of this plot, F<sub>0</sub> and F represents the fluorescence intensity in the absence and presence of quenchers. Additionally, x axis indicates the concentration of quenchers such as [I<sup>-</sup>] and [Cu<sup>2+</sup>].

While the negatively charged quencher [I<sup>-</sup>] had 220 pm ionic radius the one with positively charged quencher which is [Cu<sup>++</sup>] had 73 pm. Silica nanoparticles by I<sup>-</sup> and Cu<sup>++</sup> were less affected than free FITC according to Stern-Volmer graph. Therefore, we can say that fluorescent molecule were protected by the surrounding silica network cause good photostability. When Cu<sup>++</sup> used as quencher, more reduction in fluorescence intensity was observed in terms of free FITC. As the ionic radius of [Cu<sup>++</sup>] is smaller than negatively charged quencher [I<sup>-</sup>], it is easier to reach dye conjugate and result in quenching.

The FTIR spectra of synthesized (-) silica nanoparticles and also the particles assisted by TMAC were given in Figure 2.17. Typically, there is a silanol and silicon alkoxide groups between 400 cm<sup>-1</sup> and 1200 cm<sup>-1</sup>. IR peaks located at 800 and 1050 cm<sup>-1</sup> corresponds to Si-O-Si stretching and the band at 940 cm<sup>-1</sup> corresponds to bending modes of Si-O-H and Si-O. The peak in 3200-3500 cm<sup>-1</sup> attached to stretching modes of O-H groups. New peaks appear in the range of 2800-3100 cm<sup>-1</sup> and 1250-1500 cm<sup>-1</sup> corresponds to N-H stretching/ bending present in TMAC-assisted SiNPs which was shown as red dash in the FTIR spectrum. The blue dash presents the only TMAC chemical, so it was used as a reference. According to amine group bonding, we could say TMAC functionalization of SiNPs was done successfully.

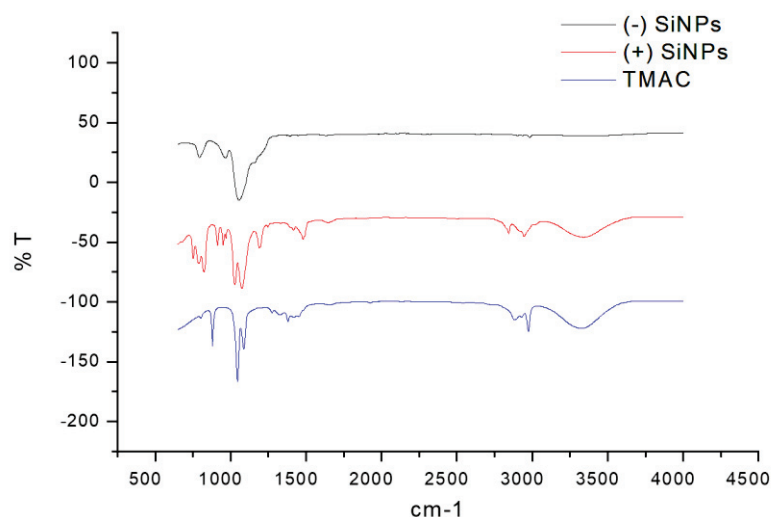


Figure 2.17. FTIR spectra of (-) and (+) potential silica nanoparticles.



SEM images were taken to characterize the surface morphology and particle size of synthesized both SiNPs (Figure 2.18-2.19.). As synthesized (-) SiNPs have small particle size, STEM technique was applied, thus the imaging capability was extended. The synthesized two silica nanoparticles have different sizes related to Scanning Electron Microscope and Scanning Transmission Electron Microscope. SEM generally gives the smaller particle size than DLS, because it measures the size in terms of hydrodynamic radius of particles. STEM-in-SEM images yielded the monodisperse size distribution of (-) potential SiNPs in 50.000-200.000 magnification and 15.00 kV for dark field and bright field mode (Figure 2.18.). SEM images of (+) potential SiNPs were shown in Figure 2.19 in 200.000 magnification with 20.00 kV.

Table 2.2. Energy Dispersive X-Ray Spectroscopy analysis of (-) SiNPs.

Element	Wt%	Atomic %
C	20.73	29.42
O	49.00	52.20
Si	30.27	18.37
Total:	100.00	100.00

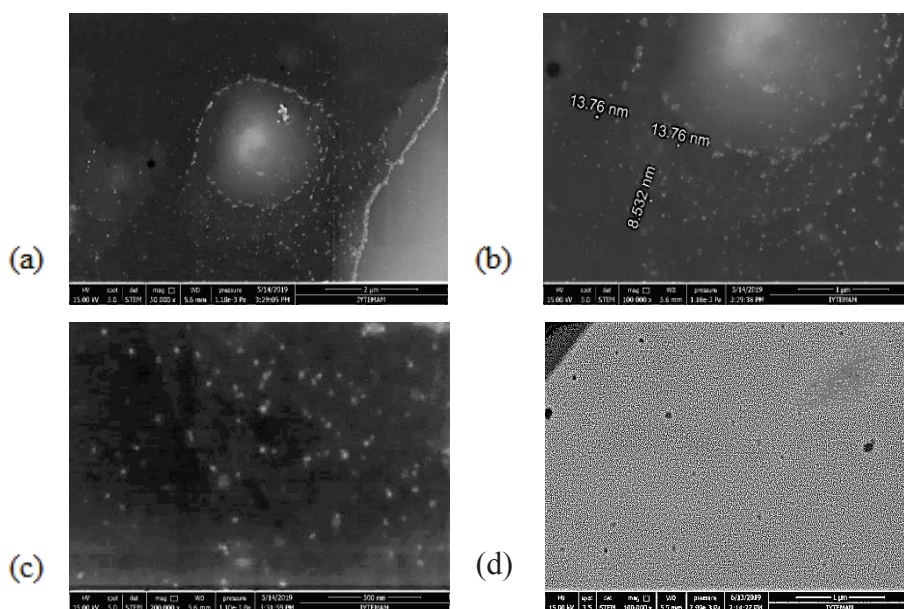


Figure 2.18. STEM images of dark field of (-) SiNPs (a) in 50.000 magnification, (b) in 100.000 magnification and (c) 200.000 magnification, bright field of fluorescent SiNPs (d) in 100.000 magnification.

EDX is the essential part of SEM which helps us to determine structural composition and quantity of particles. Table 2.2-2.3 indicates the EDX results of (-) SiNPs and (+) SiNPs. Negative potential SiNPs was composed of silicon (30.27%), oxygen (49%) and carbon (20.73%) atoms. Carbon atoms comes from the dye conjugate which provides fluorescence ability to our silica nanoparticles. The results of EDX also show the composition of silica in (-) SiNPs that was similar with (+) SiNPs; however the difference of SiNPs after TMAC conjugation was observed in the elements of nitrogen (5.26%).

Table 2.3. Energy Dispersive X-Ray Spectroscopy analysis of (+) SiNPs.

Element	Wt%	Atomic %
C	32.13	41.14
N	5.26	5.78
O	45.86	44.09
Si	15.11	8.28
Cl	1.64	0.71
Total:	100.00	100.00

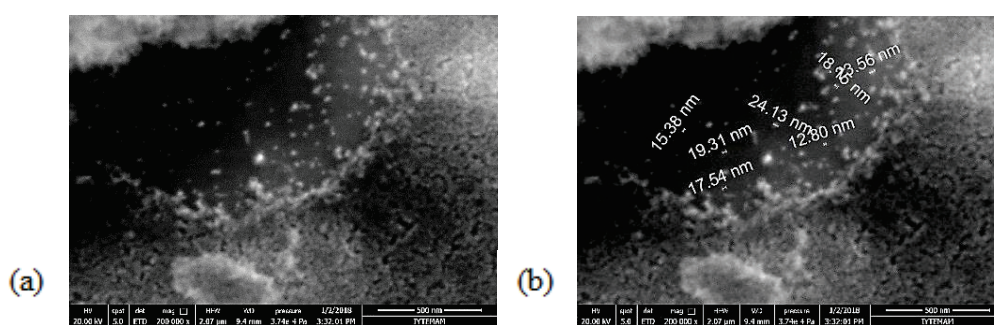


Figure 2.19. SEM images of (+) SiNPs (a), (b) in 200.000 magnification.

## 2.4. Conclusion

We demonstrated that the preparation of (-) potential silica nanoparticles and how to change the surface of that silica nanoparticles with TMAC was produced by Stöber method. Also, we reported the characterization of the both nanoparticles was performed with the help of various techniques. Dynamic light scattering method was used to get information about the particle size and surface potential of both silica nanoparticles. The particle size of (-) SiNPs and (+) SiNPs were 10 nm and 20 nm, respectively. The surface potential of (+) SiNPs was greater than (-) SiNPs. Spectrofluorometer gave us the absorbance and emission spectrum of silica nanoparticles at 495 nm and 515 nm. In order to understand the protection of FITC dye by networking silica nanoparticles, spectrofluorometer was applied. In the field of that instrument, pH, solvents and quench effects were analyzed. It is found that dye was protected by synthesized silica nanoparticles. Fourier transform infrared spectroscopy was useful to detect functional groups of silica nanoparticles. Peaks in the spectral range at around of  $400\text{ cm}^{-1}$  and  $1200\text{ cm}^{-1}$  are attributed to silica nanoparticles. Additionally, in the range of  $2800\text{-}3100\text{ cm}^{-1}$  and  $1250\text{-}1500\text{ cm}^{-1}$  corresponds to TMAC functionalized SiNPs.

Scanning electron microscope and scanning transmission electron microscope were used to generate high resolution images of samples. Both (-) and (+) potential SiNPs were analyzed by SEM and STEM to characterize the surface morphology and particle size. EDS was an analysis tool of SEM that provides the elemental analysis in our composition. Silicium and oxygen ratio were found as 30.27% and 49% for (-) potential SiNPs. The nitrogen atom was found in (+) potential silica nanoparticles with 5.26%. STEM has both bright-field and dark field mode, so the images were taken in two ways. Taking into account the size of (-) potential silica nanoparticles, STEM technique was more preferable in contrast to SEM. The images were taken in bright field and dark field mode. In bright field mode, the regions with samples are darker, while in dark field mode these regions are brighter.

## CHAPTER 3

### PARTICLE-CELL INTERACTION

#### 3.1. Introduction

##### 3.1.1. Cell Lines

In this chapter, we investigate the effects of synthesized both (-) SiNPs and (+) SiNPs on cells that are A549 (Human lung cancer cell lines) and BEAS-2B (Human lung normal cell lines).

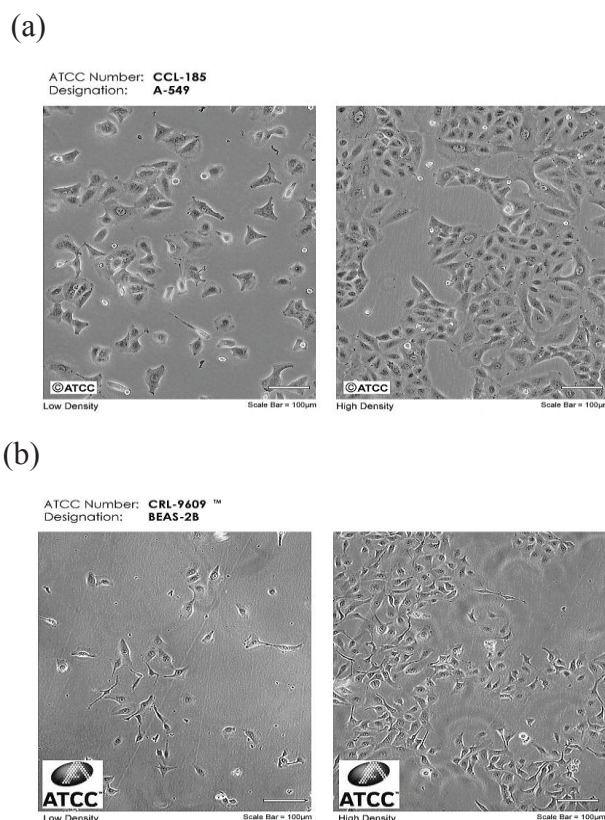


Figure 3.1. Morphology of (a) A549 and (c) BEAS-2B at low density and high density.<sup>53</sup>

Morphology of A549 and BEAS-2B cell lines were shown in Figure 3.1.<sup>53</sup> Cell morphology depends on the density and it can be explained with the cell viability. The cells that have high density is tends to the apoptosis which forms of cell death.<sup>54</sup>

The statistics of cancer types have play a significant role choosing the cell lines. According to statistics results, it can be seen the lung cancer is the most common form of cancer type for both women and men in 2018. Additionally, lung cancer has highest rates of diagnosed in new cases for both in Turkey and Worldwide. (Table 3.1. and Figure 3.2.)<sup>55,56</sup>

Table 3.1. Statistics of common types of cancer globally.<sup>55</sup>

Rank	Cancer	New cases diagnosed in 2018	% of all cancers (excl. non-melanoma skin cancer)
	All cancers*	17,036,901	
1	Lung	2,093,876	12.3
2	Breast	2,088,849	12.3
3	Colorectal**	1,800,977	10.6
4	Prostate	1,276,106	7.5
5	Stomach	1,033,701	6.1
6	Liver	841,080	5.0
7	Oesophagus	572,034	3.4
8	Cervix uteri	569,847	3.3
9	Thyroid	567,233	3.3
10	Bladder	549,393	3.2
11	Non-Hodgkin lymphoma	509,590	3.0
12	Pancreas	458,918	2.7
13	Leukaemia	437,033	2.6
14	Kidney	403,262	2.4

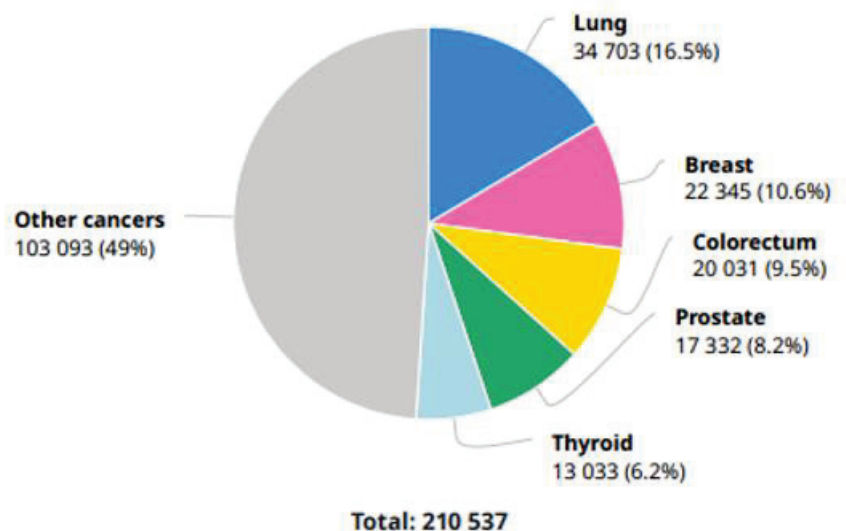


Figure 3.2. Statistics of cancer types for new cases diagnosed in Turkey, 2018.<sup>56</sup>

### 3.1.2. Cell Viability

MTT [3-(4,5-dimethylthiazol-2-yl)-2,5-diphenyltetrazolium bromide] is type of colorimetric assay that frequently used to assessing cell viability and cytotoxicity. MTT assay was first described by Mossman in 1983. In colorimetric assay, mitochondrial dehydrogenase enzymes reduce the yellow color MTT to purple-colored dye formazan product. In the presence of living cell, MTT is converted to formazan.<sup>57</sup> The structures of MTT and formazan were shown (Figure 3.3.).

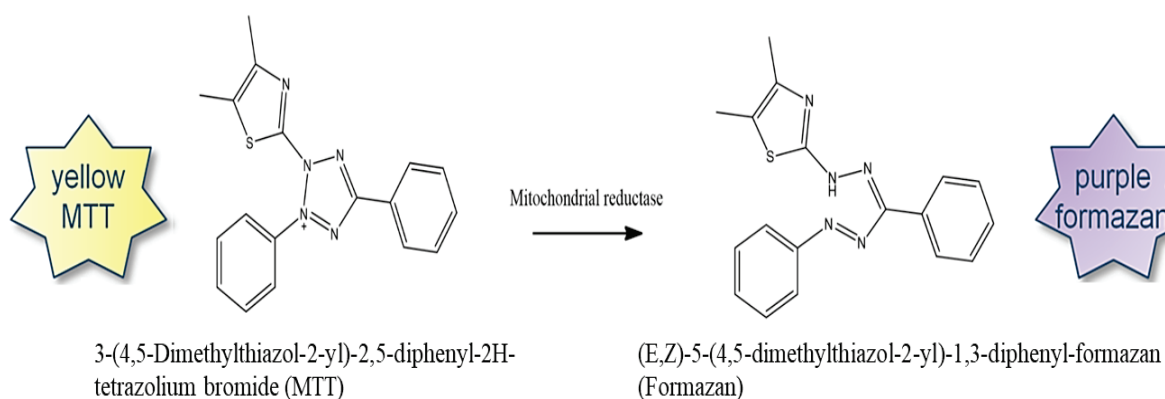


Figure 3.3. Enzymatic reduction of MTT to formazan.

### 3.1.3. Staining of Mitochondria

In cellular function, organelles play a crucial role in the maintenance of identify targets of interest in cells. Mitochondria are critical to cell life with its two distinct properties; which are adenosine triphosphate(ATP) production and cell death mechanism regulation.<sup>58</sup> Therefore, visualization of mitochondria will be significant. To achieve that goal, Mito Red was used. It is type of a far-red fluorescent dye with the excitation and emission value were found at 581 nm, 644 nm, respectively. At the end of the mitochondria staining, fixation procedure was applied. The one of the reason of fixation was preserving the cells components in life-like-state.<sup>59,60</sup> The another reason was if no time to analyze biological sample, then fixation becomes preferable option. Mito Red is cell permeable probes that contain thiol-reactive chloromethyl moiety. The chloromethyl group seems to be in charge of keeping the dye and mitochondria together after fixation process.<sup>61</sup>

### 3.1.4. Mitochondrial Membrane Potential

Mitochondrial membrane potential ( $\Delta\Psi_m$ ) is the main driving force for ATP synthesis. The basic process of mitochondrial membrane potential were indicated (Figure 3.4.).<sup>62</sup> It is significant marker for cellular metabolic activity such as electron transport and oxidative phosphorylation. Oxidative phosphorylation is made up of two connected components; the electron transport chain and chemiosmosis. The electron transport chain is a series of proteins and organic molecules found in the inner membrane of the mitochondria. Electrons are passed from one member of the transport chain to another in a series of redox reactions. For example, NADH is very good at donating electrons in redox reactions, so it can transfer its electrons directly to complex, turning back into  $\text{NAD}^+$ . Energy released in these reactions is captured as a proton gradient. In chemiosmosis, the energy stored in the gradient is used to make ATP.<sup>63</sup>

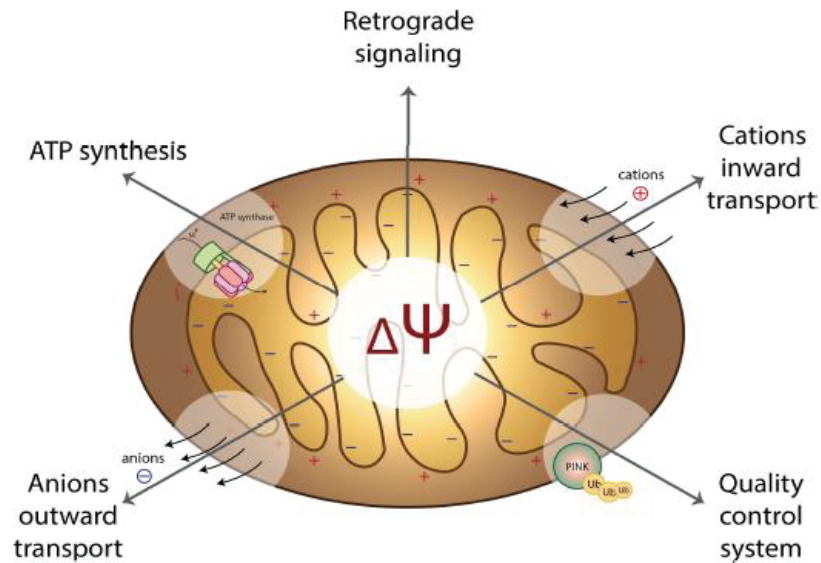


Figure 3.4. The diagram of mitochondrial membrane potential.<sup>62</sup>

### 3.1.5. Confocal Microscopy

Confocal microscopy is a powerful technique to explain the visualization morphology of biological samples.<sup>64</sup> It was pioneered by Marvin Minsky in 1957.

The laser scanning confocal microscope experimental set-up was given (Figure 3.5).<sup>65</sup> This process works as follows: intensity of light source increases by using laser light source. Thus, we can get better image in a way of contrast and resolution. Confocal microscopy includes two confocal aperture which is called as pinhole. It has very small diameter, so very less number of laser light can pass through the pinhole. Then, the laser light goes into dichromatic mirror in which it reflects the light to the condenser. After that, the light is reflected to the biological specimen or sample. The sample is diverted through the objective lens to the detector. In that case, the second pinhole where the light is shown as red light is located in out of focus light rays and they are stopped. The light which is coming specifically through a particular point of the sample is diverted toward to photomultiplier (PMT) detector. The reason of using PMT is because it has capability to detect very small intensity.<sup>66</sup>



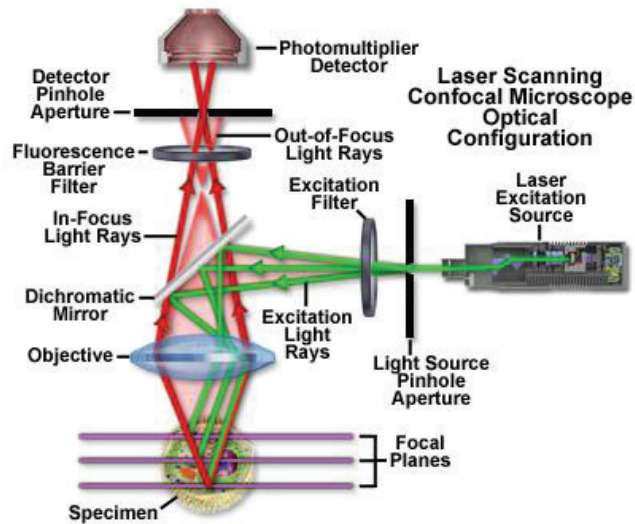


Figure 3.5. Laser scanning confocal microscopy set-up.<sup>65</sup>

Spinning disk confocal microscopy is another types of confocal microscopy. The spinning disk confocal system brings new possibilities that making image more effective in contrast to scanning system. Spinning system has multiple pinholes that allowing much sensitive illumination and reduced photobleaching. These pinholes are scanned across the image multiple times per exposure and every part of the image is scanned by a pinhole each 30 degree rotation of the disk. It can be acquired up to two thousand frames per second by multi-point scanning by regulating the disk rotation speed.<sup>67</sup>

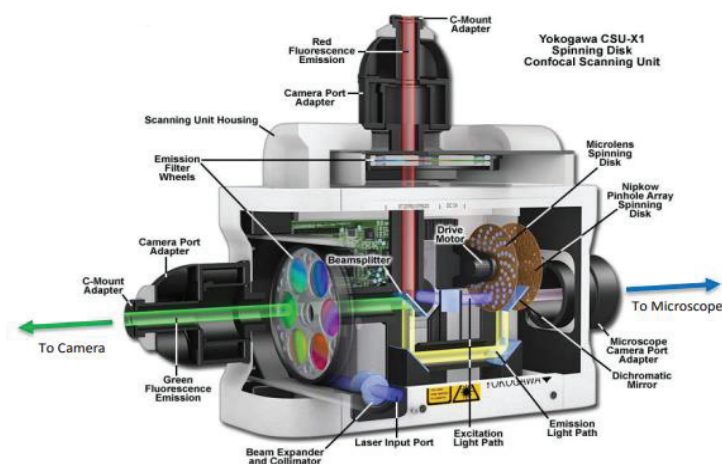


Figure 3.6. Spinning disk confocal microscopy set-up.<sup>67</sup>

### 3.1.6. Colocalization Analysis

Confocal microscopy is also provide the colocalization analysis. It is estimated using algorithms that calculate coefficients such as Pearson's correlation coefficient (PCC). In this way, we can obtain colocalization quantitatively. The formula of Pearson's correlation was given as follows;

$$r = \frac{\sum_i(x_i - x_{ave})(y_i - y_{ave})}{\sqrt{\sum_i(x_i - x_{ave})^2} * \sqrt{\sum_i(y_i - y_{ave})^2}} \quad (1.4)$$

where  $x_i$  and  $y_i$  represents the intensities of the red and green channels;  $x_{ave}$  and  $y_{ave}$  display the average intensities of these channels. The range of PCC value is from -1.0 to 1.0, where 0 exhibits no significant correlation and -1.0 exhibits negative correlation. When the coefficient approaches 1.0 that means there is relation between variables. For  $r=1.0$ , it can be said that total positive correlation.<sup>68</sup>

## 3.2. Experimental

### 3.2.1. Materials

DMEM High Glucose (Dulbecco's Modified Eagle Medium), FBS (Fetal Bovine Serum), Pen-Strep (penicillin streptomycin), RPMI 1640 (Roswell Park Memorial Institute), trypsin EDTA were taken from Biological Industries (BI) for cell culture study.

4 % paraformaldehyde (PFA) was used for cell fixation.

Mito-Tracker Red was used to staining mitochondria in cells.

MTT (3-(4,5-Dimethylthiazol-2-yl)-2,5-Diphenyltetrazolium Bromide) assay was used to determine whether the viability of nanoparticle-treated cells.

### **3.2.2. Instrumentation**

Memmert INC 108 CO<sub>2</sub> incubator and Esco Laminar Cabinet were used to cultivation of cells. Memmert WNE7 waterbath were frequently used to continue of the cells.

Olympus IX71 Spinning Disk Confocal Microscope (Andor Revolution) was applied in order to cell imaging. The images were taken using BF (Bright Field). The 40x objective lens and 100x oil-immersion objective lens were used for fixed cell depending on experimental necessity.

MTT assay were read out by Varioskan Flash Spectroscopy (Thermo ) after centrifugation process by HETTICH ROTINA 38R in Izmir Institute of Technology-IZTECH, Biotechnology and Bioengineering Research and Application Center.

### **3.2.3. Cell Cultivation**

A549 and BEAS-2B which are basis of human lung carcinoma epithelial and human bronchial epithelial cell lines were used to checking activity of synthesized silica nanoparticles. To maintain cell culture, sterile environment in which RPMI 1640, DMEM High Glucose contains 10% FBS, %1 penicillin and %1 L-glutamine can be provided at 37 °C in a 5% CO<sub>2</sub> incubator.

### **3.2.4. Cell Imaging**

Cells exposed to engineered (-) SiNPs (20µg/ml) and (+) SiNPs (20µg/ml) to determine the localization of nanoparticles by imaging with confocal microscopy. The specimen was plated on sterile coverslips in 6-well plates.

Initially, the media which was treated with NPs should be washed with PBS solution. Then, A549 and BEAS-2B cells were stained by 200nM of Mito-Tracker Red (Sigma Aldrich) with incubation time as 30 minutes. After the incubation, the medium was removed from the wells and washed with PBS two times. 3.7% paraformaldehyde (PFA) was used to fixation of cells for 10 minutes.

After the fixation, the medium was washed with PBS three times carefully. The PBS medium was replaced with the ethanol by applying ethanol gradation using 30%, 50%, 70% and 100%. The solution was kept at +4C°.

To get information about the fixed-cell imaging the slides were removed from the wells. The nail polish was put four corners to anchor coverslip. Slides were letting dry for about two minutes. We analyzed the slides with the help of confocal microscope. Our confocal spinning disk electron microscopy consist of the Inverted microscope (Olympus IX-71), Andor Revolution Imaging System, Stage incubator system (Okolab), The optical working table for vibration (Newport), The CCD camera works in 15-200 fps (Andor), Piezoelectrical set-up, AOTF photon regulator (Andor) and 4 lasers in 405, 488, 532, 640 nm wavelength.

To obtain emissions of F-SiNPs and stained mitochondria 488 nm and 532 nm were utilized, respectively.

### **3.2.5. Cytotoxicity**

To determine potential cytotoxic effects of the fluorescent silica nanoparticles, colorimetric assay (MTT based) was managed for 96-well plates. The absorbance of this solution can be measured in the range of 500-600 nm by a spectrophotometer. Initially, 300.000 cell/ml were seeded in each plate containing final volume of 100  $\mu$ l/well. Mediums were removed after 24h and then silica particles treated with four different concentrations (0.2 $\mu$ l, 2 $\mu$ l, 20 $\mu$ l and 200 $\mu$ l). The incubation period for the assay were 24, 48 and 72 hours to identify cellular viability of SiNPs treated-cells. After incubation, cells were washed with phosphate-buffered saline. MTT solutions were added per well and incubate 37° for 3 hours. Centrifugation procedure was started through 10 minutes at 1800 rpm. As DMSO was suitable solvent for dissolving the formazan, it was added after centrifugation. After these processes, cytotoxic potential of particle treated cells were measured at 540nm.

### 3.3. Results and Discussion

#### 3.3.1. MTT Assay

Cell viability was assessed for A549 and BEAS-2B cell lines using engineered both (-) SiNPs and (+) SiNPs. Both cells were exposed to nanoparticles with different doses (0.2  $\mu\text{g/ml}$ , 2  $\mu\text{g/ml}$ , 20  $\mu\text{g/ml}$  and 200  $\mu\text{g/ml}$ ) in 24, 48 and 72 h incubation periods. The control group that means untreated with synthesized silica nanoparticles was used to validate results of the experiment.

It was found that the cell viability was both dose- and time-dependent. In all cases, the minimum viability was found for 200  $\mu\text{g/ml}$  and at 72 h. It could be viewed that time and dose affected in direct proportion to toxicity of cells.<sup>69,70</sup>

As stated by MTT assay, cell viability rate of dose (20  $\mu\text{g/ml}$ ) was found 77% in 24 h and 75% in 48 h for (-) SiNPs treated A549 cell. The value was decreased up to 74% in 24 h and 57% in 48 h for (+) SiNPs treated with A549. In lung normal cell line, survival rate of (20 $\mu\text{g/ml}$ ) dose was detected 82% in 24 h and 72% in 48 h for (+) SiNPs exposed BEAS-2B cell line. The viability rate of (-) SiNPs exposed BEAS-2B was much lower in 48h (49%) compared to 24 h (83%) (Figure 3.7-8).

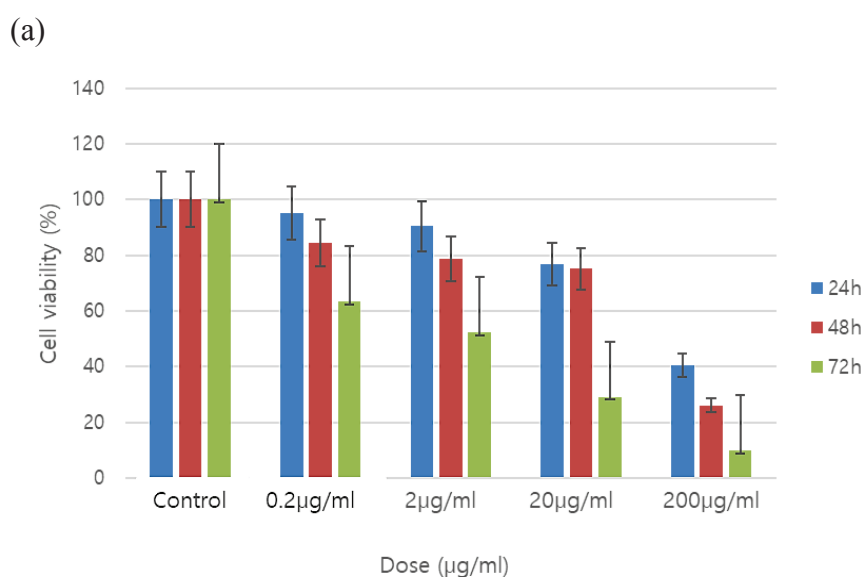


Figure 3.7. (Cont. on next page)

(b)

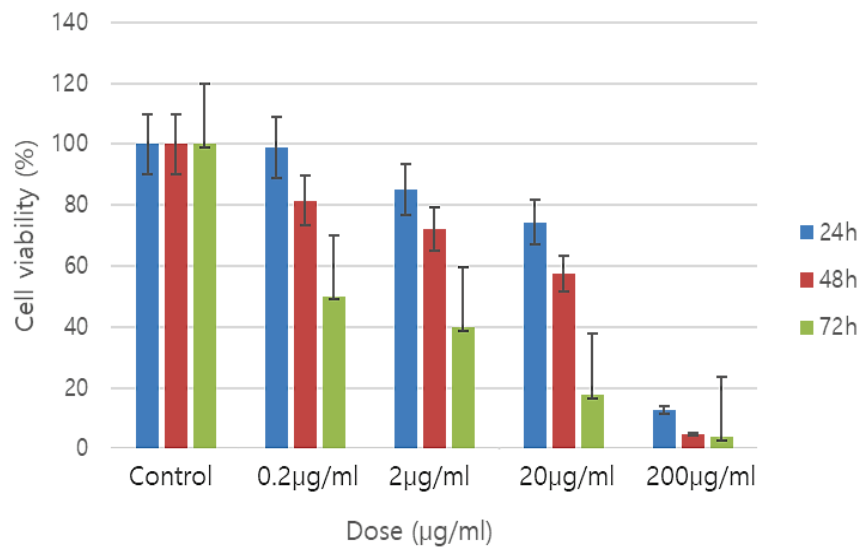


Figure 3.7. The schematic representation of MTT assay of (a) (-) SiNPs and (b) (+) SiNPs for A549 cell line.

(a)

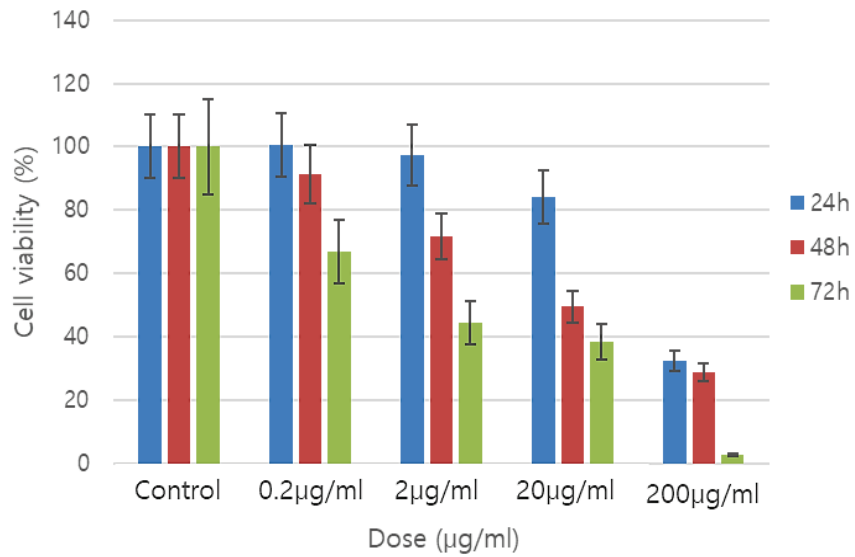


Figure 3.8. (Cont. on next page)

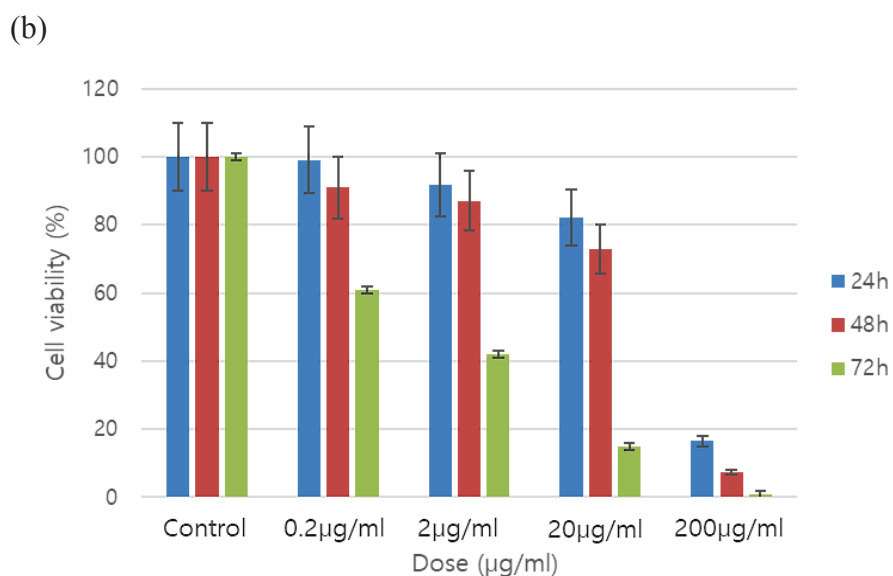


Figure 3.8. The schematic representation of MTT assay of (a) (-)SiNPs and (b) (+) SiNPs for BEAS-2B cell line. (Cont.)

### 3.3.2. Confocal Imaging

Confocal microscopy was used to verify the location of negative potential SiNPs (20 $\mu\text{g/ml}$ ) and positive potential SiNPs (20 $\mu\text{g/ml}$ ) to mitochondria. For this purpose, mitochondria was stained with the Mito-Red. The images were generated with using 40x (intermediate magnification) and 100x (high magnification) objective lens.

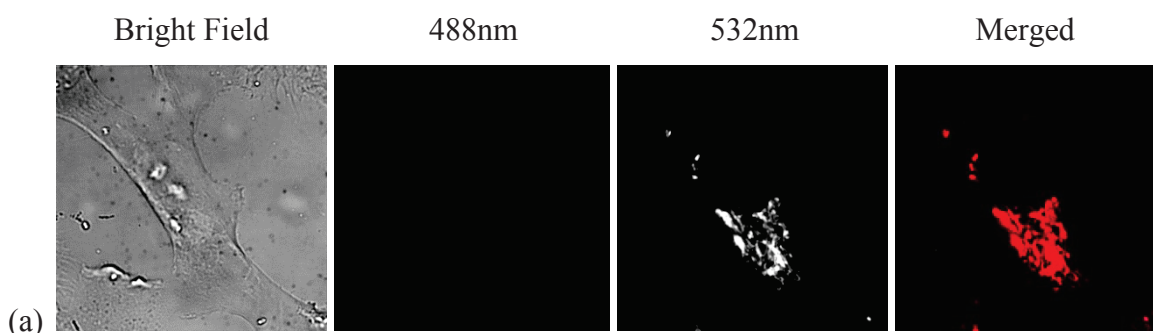


Figure 3.9. (Cont. on next page)

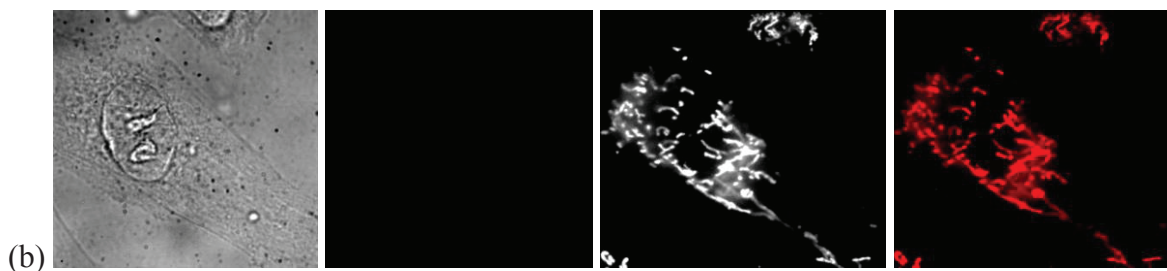


Figure 3.9. Confocal images of control group for (a) A549 cell line and (b) BEAS-2B cell line using 100x objective. (Cont.)

Initially, we took the images of control groups for both cell lines in a bright field mode. The 488 nm (emission filter) was responsible for the silica nanoparticles. Thus, we could not see images in 488 nm for control group (Figure 3.9).

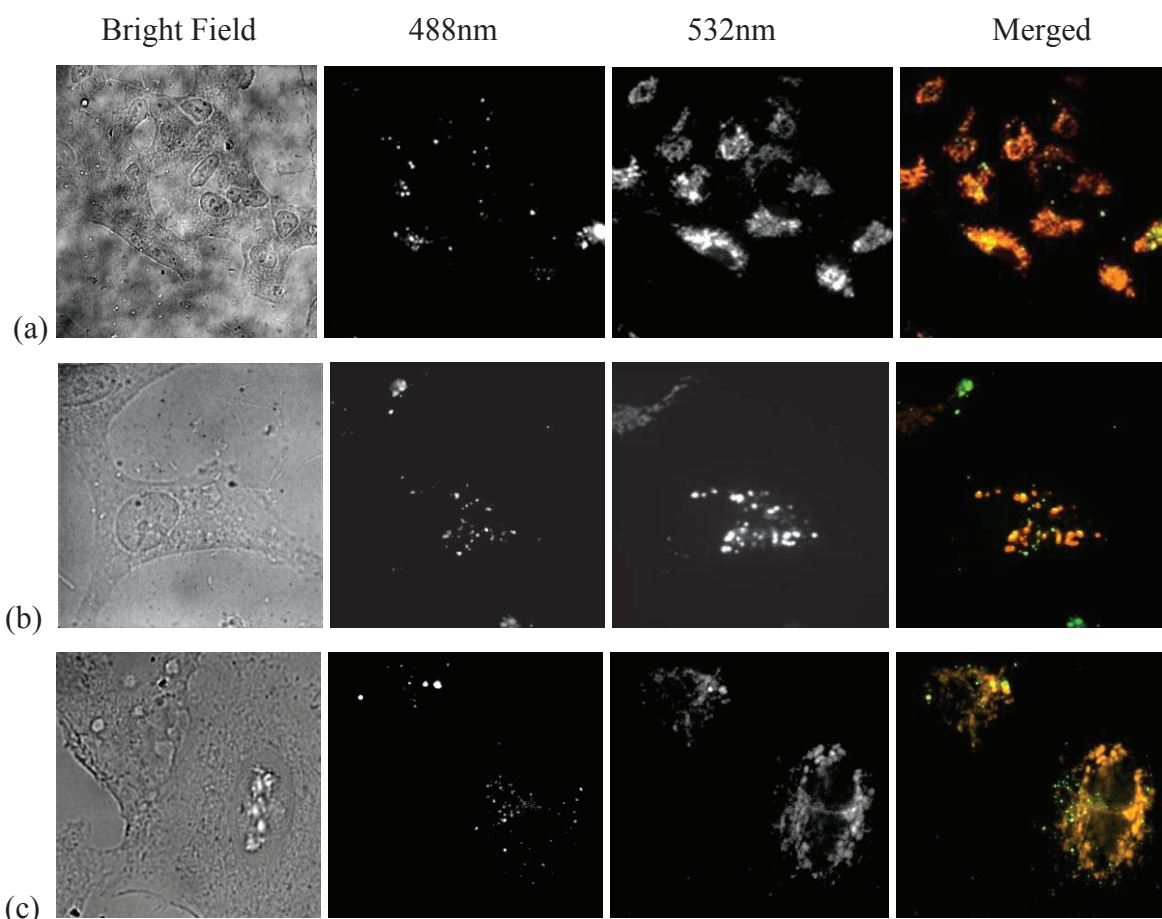


Figure 3.10. Confocal images of (-) SiNPs-treated with A549 cell line for (a) 40x and (b), (c) 100x objective.



Mitochondria was seen using emission filter which was 532 nm. The all merged images were seen as red, because the only variable here Mito-Red.

Negative potential SiNPs and positive potential SiNPs-treated with A549 cell were given (Figure 3.10,11.). Bright field were taken in order to observe general images of the cell. The particles were well distributed throughout the cell that seen at 488 nm. The mitochondria was induced by 532 nm laser as red color. In the merged images, green color represent the our nanoparticles. It can be seen yellow color after merging of green (488nm) and red channels (532nm). The yellow color was more apparent in the (+) SiNPs than (-) SiNPs.

The green fluorescence of both (-) SiNPs and (+) SiNPs located in BEAS-2B cells (Figure 3.12,13.). The interaction between particles and the lung normal cell were observed well-distributed.

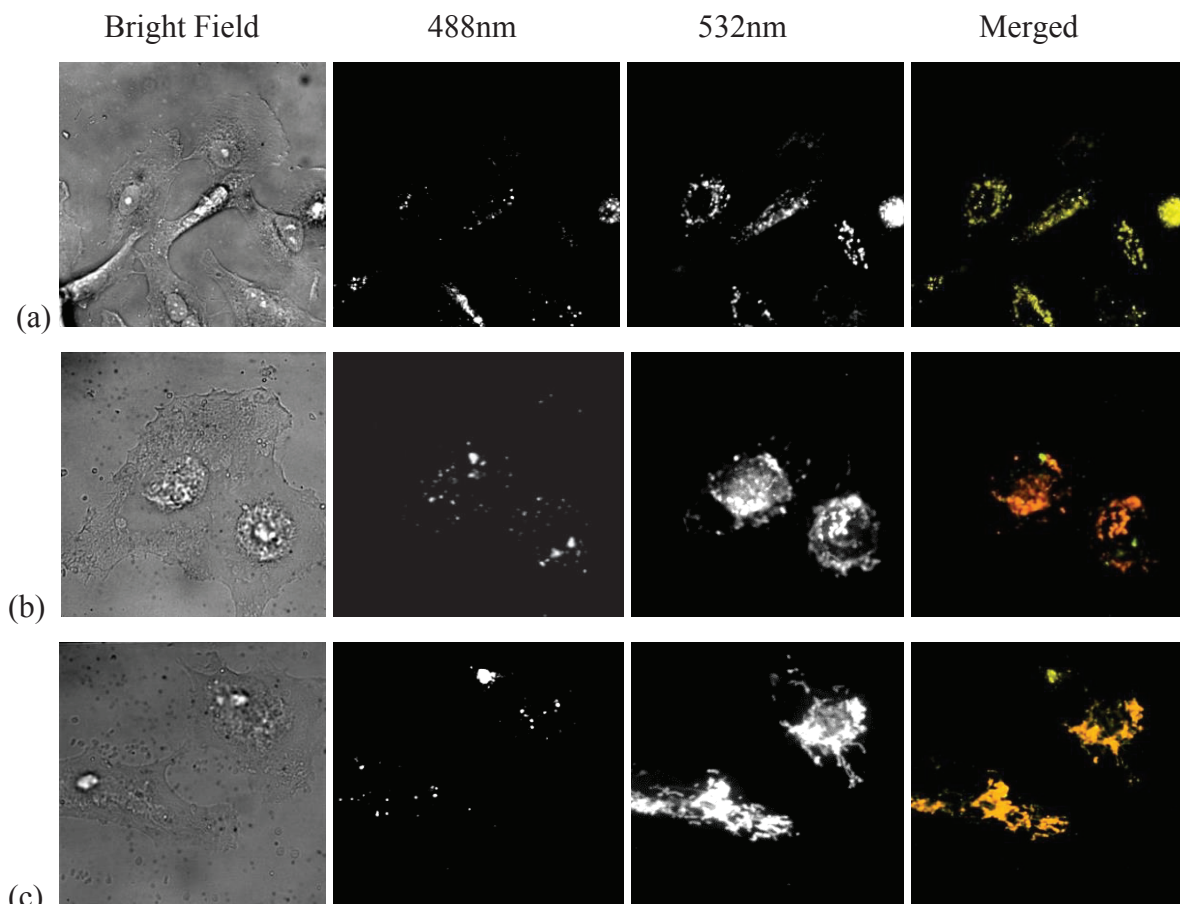


Figure 3.11. Confocal images of (+) SiNPs-treated with A549 cell line for (a) 40x objective and (b), (c) 100x objective.

Results in Figure 3.11,12. were shown that the green color partly merge with red color for (+) potential SiNPs. Yellow spots in the overlay pictures were seen better in (-) potential SiNPs compared to (+) potential SiNPs.

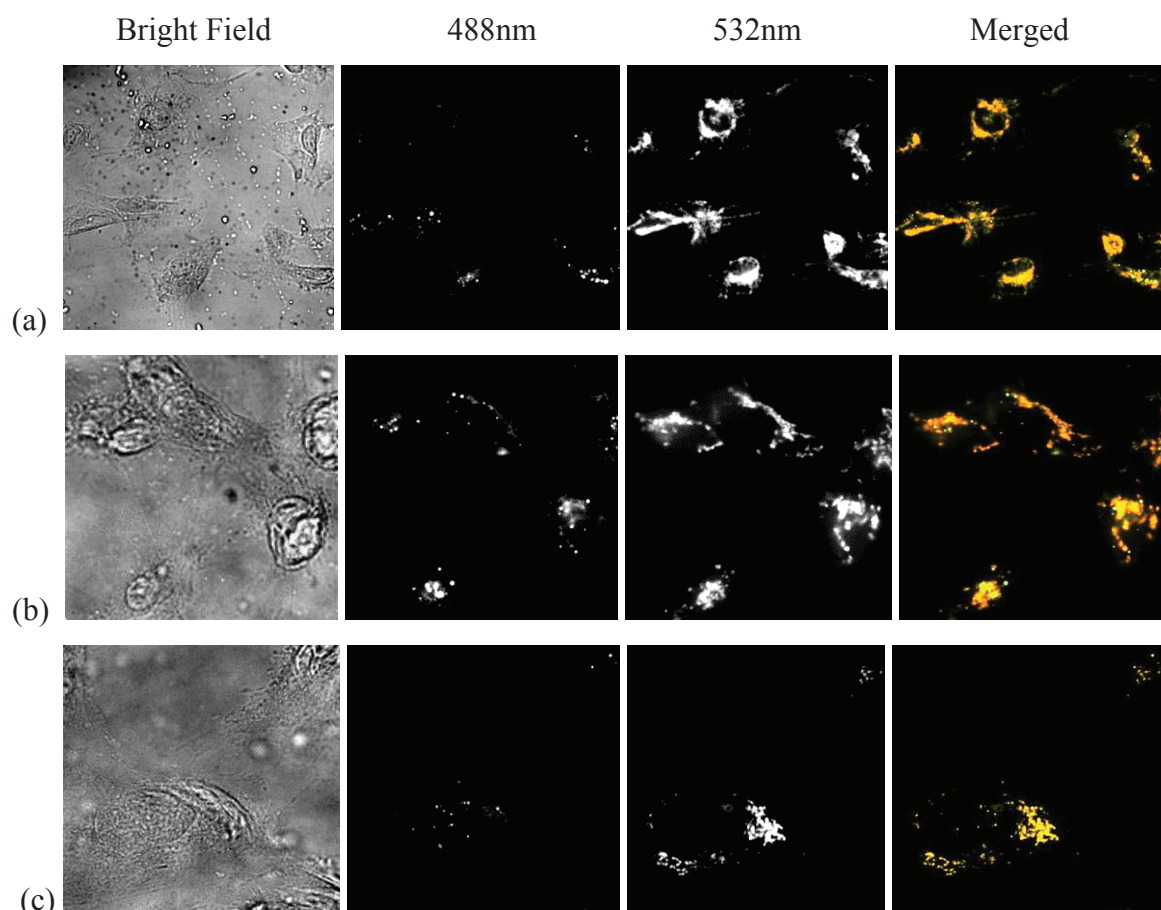


Figure 3.12. Confocal images of (-) SiNPs-treated with BEAS-2B cell line for (a) 40x objective and (b), (c) 100x objective.

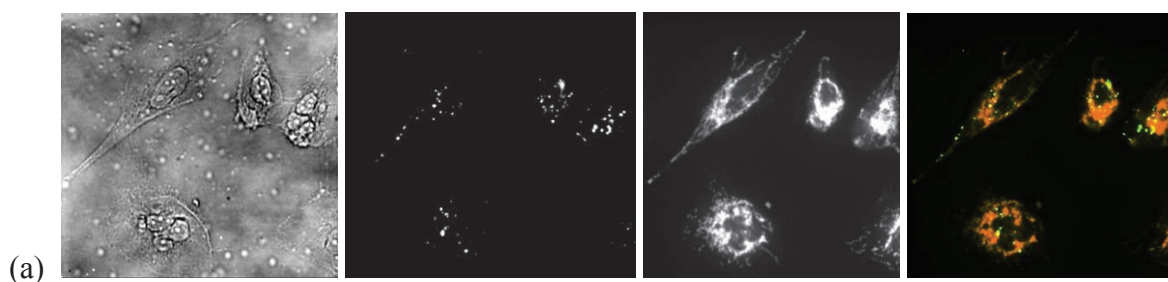


Figure 3.13. (Cont. on next page)

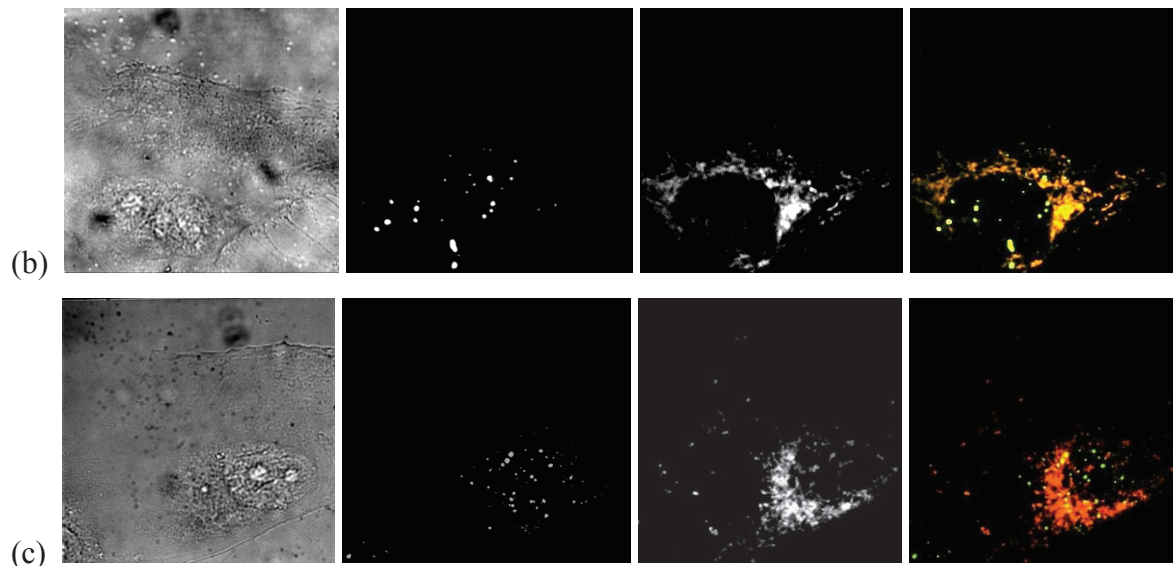


Figure 3.13. Confocal images of (+) SiNPs-treated with BEAS-2B cell line for (a) 40x objective and (b), (c) 100x objective (Cont.)

### 3.3.3. Colocalization Analysis

To quantified overlap degrees of synthesized particles, co-localization process was applied using Pearson's coefficient correlation. The images were analyzed by Image J Coloc-2 plug-in.

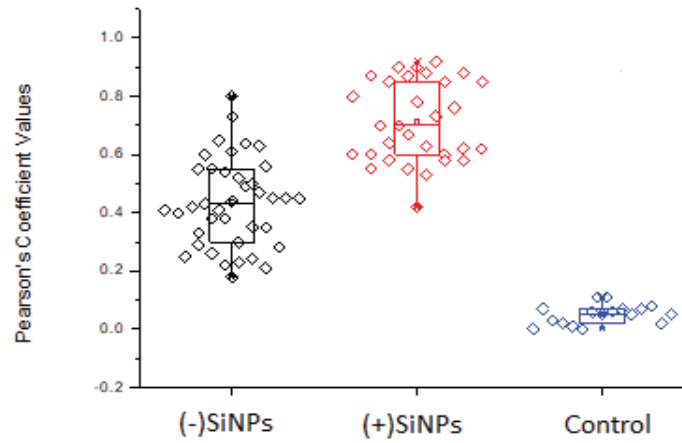
The colocalization measurements were processed with the control group to understand exact effects of engineered particles. According the correlation value, there was not observed colocalization between the control groups and mitochondria, that's what was expected.

(+) SiNPs were more colocalized than (-) SiNPs in A549 cell. (Figure 3.14,a). In a typical cell, mitochondrial membrane potential is highly negative (approximately -180mV) due to chemiosmotic gradient of protons which is used to make ATP.<sup>71</sup> Therefore, the zeta potential of (+) SiNPs can be relevant to explain colocalization analysis for A549 cell.

Based on results of colocalization studies for BEAS-2B, (+) SiNPs were less colocalized than A549. This can be accounted for in part by hyperpolarization. It is related to changing of cell's membrane potential which makes it more negative.

Typically, mitochondrial membrane potential of cancer cells ( $\Delta\Psi_m = \approx -220\text{mV}$ ) have more hyperpolarised than potential of normal cells ( $\Delta\Psi_m = \approx -140\text{mV}$ ).<sup>72</sup>

(a)



(b)

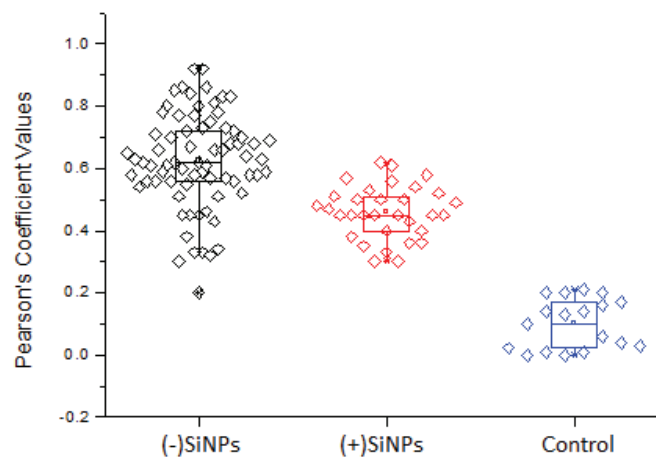


Figure 3.14. Distribution of pearson coefficients of (-) SiNPs, (+) SiNPs and Control group for A549 and (b) BEAS-2B cell.

We also applied the statistical test to determine whether the result of data was statistically different. The test results indicated the  $p < 0.05$ , that means variables were

statistically significant. Following this, t-test was used to compare the means of two populations. We obtained the absolute value of t-value was greater than the critical value. Therefore, the null hypothesis is rejected, the effect is said to be statistically significant.<sup>73</sup>

### 3.3.4. Mitochondrial Intensity Analysis

Mitochondrial intensity analysis was used to estimate mitochondrial activity of both nanoparticles for A549 and BEAS-2B. Regions of interest (ROI) which have ability to select pattern on specific image regions were used to identify analysis.

(+) SiNPs treated with A549 tends to increased their area (Figure 3.15.), which can be explained with the loss of energy production in the cell. ATP production is concerned with the cell life and death. There are two distinctive forms of cell death such as early apoptosis and late apoptosis/necrosis. Apoptosis is the most common form of programmed cell death. Concerning the necrosis, the cell death mechanism based on unregulated that is form of cell injury.<sup>74,75</sup> The behavior of (+) SiNPs in A549 cell could be explained with the late apoptosis. It can be said that mitochondrial function of A549 was affected by (+) SiNPs.

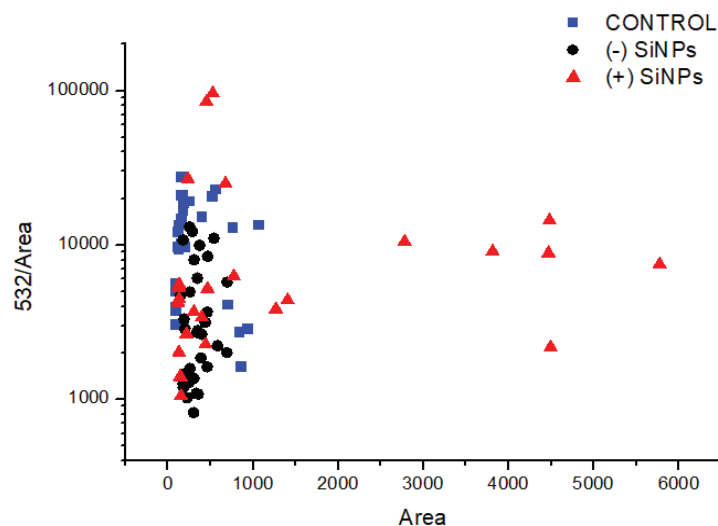


Figure 3.15. Mitochondrial intensity analysis of (-) SiNPs, (+) SiNPs and Control group for A549 cell line.

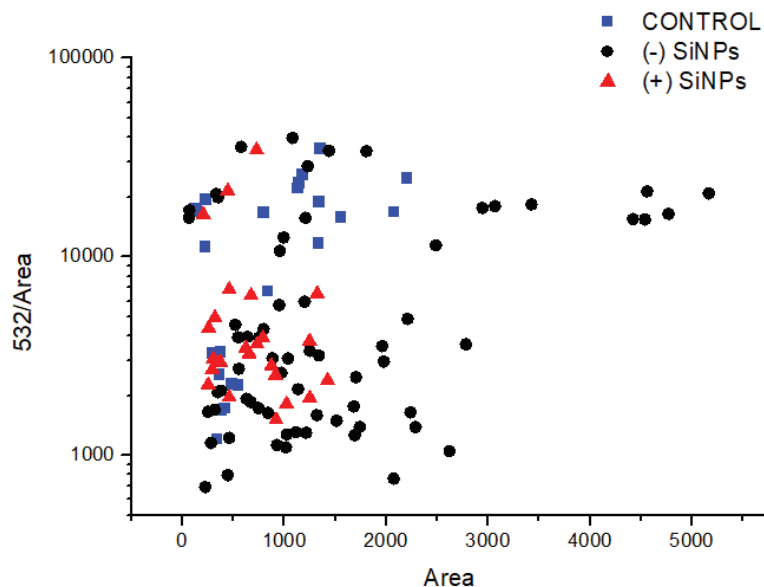


Figure 3.16. Mitochondrial intensity analysis of (-) SiNPs, (+) SiNPs and Control group for BEAS-2B cell line.

In Figure 3.16., the tendency of increasing area was more apparent in (-) SiNPs rather than (+) SiNPs in BEAS-2B cell line. Thus, mitochondria in the BEAS-2B cell was more affected by (-) potential SiNPs instead of (+) potential SiNPs.

Despite the area of cells were affected, the mitochondrial intensity of cells were not changed after silica nanoparticles treatment compared to control group.

### 3.4. Conclusion

Altogether, we investigated the effects of (-) potential silica nanoparticles and (+) potential silica nanoparticles on the A549 cell and BEAS-2B cell lines. In biological applications, to understand toxicological behavior of SiNPs, cell viability test was performed. We found that viability of both types of silica nanoparticles were dose (0.2 $\mu$ g/ml to 200 $\mu$ g/ml) and time (24h,48h,72h) dependent. In this study, 20 $\mu$ g/ml dose was selected according to MTT assay results. To determine location of synthesized silica nanoparticles, spinning disk confocal microscopy was used with 40x and 100x objective lens. The emission filter of 488 nm (green channel) was responsible for the silica nanoparticles. Mitochondria was identified with the 532 nm, which stands for red channel. When images of 488 nm and 532 nm were overlaid the yellow color was seen

for silica nanoparticles. In the case of control group, yellow color was not obtained when the merged images of two channels.

Colocalization analysis were applied dependent on the Pearson's correlation coefficient. Image J Coloc-2 plug-in tool provides the colocalization analysis of captured images. According to colocalization results, (+) potential SiNPs were more colocalized in A549 than BEAS-2B cell lines. The reason of that, the mitochondrial membrane potential of cancer cell has more negative than normal cell due to hyperpolarization. To verify the significant difference of variables, statistical tests were used. The statistical results ( $p < 0.05$  and  $|t_{stat}| > t_{crit}$ ) show that there was a statistically significant difference between the mean of variables. A further implication was analysis of mitochondrial intensity. In A549 cell line, (+) SiNPs were tends to increase their area which confirms effecting the mitochondria. It was clearly seen that mitochondrial intensity of cells were not significantly affected treatment with the (-) SiNPs and (+) SiNPs compared to control group.

## CHAPTER 4

### CONCLUSION

This study aimed to identify effects of synthesized (-15mV) potential, 10nm particle size silica nanoparticles and (+30mV) potential, 20nm particle size silica nanoparticles on A549 and BEAS-2B cell lines. Based on characterization analysis of particle-cell interaction, it can be concluded that using fluorescent dye and modifying the surface of SiNPs are important factors in bio-applications.

Mainly, we synthesized both (-) and (+) potential silica nanoparticles by using modified Stöber method. Three factors such as pH, solvent and quench effects were investigated to better understand implications of fluorescent dye in silica NPs. To prevent dye leakage, FITC molecules were attached covalently to SiNPs via a stable thiourea linkage. Absorption and emission spectra of dye conjugate confirmed the successful doping of dye molecules in the SiNPs.

In cellular applications, to evaluate cytotoxicity, human lung cancer cell and human lung normal cell were exposed to both silica nanoparticles. We determined that time and dose affect the toxicity of cells in direct proportion. According to MTT assay results, (-) and (+) SiNPs were non-toxic with the dose of 20  $\mu\text{g/ml}$  in 48h. We also demonstrated that the accumulation of SiNPs within mitochondria as stated in Pearson's Coefficient Correlation. It was found that mitochondrial intensity of A549 and BEAS-2B cells were not significantly changed after SiNPs treatment compared to control group.

Silica nanoparticles are mostly used nanomaterials due to its biocompatible nature. Surface modification of dye-doped silica nanoparticles are a promising material for biomedical areas. Further research is needed to develop the causes of relationship between surface functionalized silica nanoparticles and the cells.



## REFERENCES

1. Amin, M. T.; Alazba, A. A.; Manzoor, U., A Review of Removal of Pollutants from Water/Wastewater Using Different Types of Nanomaterials. *Advances in Materials Science and Engineering* **2014**, *2014*, 1-24.
2. Khan, I.; Saeed, K.; Khan, I., Nanoparticles: Properties, applications and toxicities. *Arabian Journal of Chemistry* **2017**.
3. Zhou, Q.; Zhang, L.; Wu, H., Nanomaterials for Cancer Therapies. *Nanotechnology Reviews* **2017**, *6*.
4. Kim, T. G.; An, G. S.; Han, J. S.; Hur, J. U.; Park, B. G.; Choi, S.-C., Synthesis of Size Controlled Spherical Silica Nanoparticles via Sol-Gel Process within Hydrophilic Solvent. *Journal of the Korean Ceramic Society* **2017**, *54* (1), 49-54.
5. Shirshahi, V.; Soltani, M., Solid silica nanoparticles: Applications in molecular imaging. *Contrast media & molecular imaging* **2015**, *10*.
6. Stober, W.; Fink, A.; and Bohn, E., Controlled Growth of Monodisperse Silica Spheres in the Micron Size Range. *Journal of Colloid and Interface Science* **1968**, *26*, 62-69.
7. Lim, J.-H.; Ha, S.-W.; Lee, J.-K., Precise Size-control of Silica Nanoparticles via Alkoxy Exchange Equilibrium of Tetraethyl Orthosilicate (TEOS) in the Mixed Alcohol Solution. *Bulletin of the Korean Chemical Society* **2012**, 1067-1070.
8. Issa, A. A.; Luyt, A. S., Kinetics of Alkoxysilanes and Organoalkoxysilanes Polymerization: A Review. *Polymers (Basel)* **2019**, *11* (3).
9. Greasley, S.; Page, S.; Sirovica, S.; Chen, S.; Martin, R.; Riveiro, A.; Hanna, J.; Porter, A.; Jones, J., Controlling particle size in the Stöber process and incorporation of calcium. *Journal of Colloid and Interface Science* **2016**, *469*.
10. Shimura, N.; Ogawa, M., Preparation of surfactant templated nanoporous silica spherical particles by the Stöber method. Effect of solvent composition on the particle size. *Journal of Materials Science* **2007**, *42* (14), 5299-5306.
11. Durgun, G.; Ocakoglu, K.; Ozcelik, S., Systematic Tuning the Hydrodynamic Diameter of Uniformed Fluorescent Silica Nanoparticles. *Journal of Physical Chemistry C* **2011**, *115* (33), 16322-16332.

12. Qi, D.; Lin, C.; Zhao, H.; Liu, H.; Lü, T., Size regulation and prediction of the SiO<sub>2</sub> nanoparticles prepared via Stöber process. *Journal of Dispersion Science and Technology* **2016**, *38* (1), 70-74.
13. Q. Zhao, I. T. Young and J. G. S. de Jong, "Photon budget analysis for a novel fluorescence lifetime imaging microscopy system with a modulated electron-multiplied all-solid-state camera," *2009 IEEE 3rd International Conference on Nano/Molecular Medicine and Engineering*, Tainan, **2009**, 104-107.
14. Burns, A.; Ow, H.; Wiesner, U., Fluorescent core-shell silica nanoparticles: towards "Lab on a Particle" architectures for nanobiotechnology. *Chem Soc Rev* **2006**, *35* (11), 1028-42.
15. Nyffenegger, R., C. Quellet, and J. Ricka, Synthesis of fluorescent, monodisperse, colloidal silica particles. *Journal of colloid and interface science*, **1993**, *159*(1), 150-157.
16. Ma, K.; Sai, H.; Wiesner, U., Ultrasmall Sub-10 nm Near-Infrared Fluorescent Mesoporous Silica Nanoparticles. *Journal of the American Chemical Society* **2012**, *134* (32), 13180-13183.
17. Grimm, J. B.; English, B. P.; Chen, J.; Slaughter, J. P.; Zhang, Z.; Revyakin, A.; Patel, R.; Macklin, J. J.; Normanno, D.; Singer, R. H.; Lionnet, T.; Lavis, L. D., A general method to improve fluorophores for live-cell and single-molecule microscopy. *Nat Methods* **2015**, *12* (3), 244-50, 3 p following 250.
18. Thiruppathi, R.; Mishra, S.; Ganapathy, M.; Padmanabhan, P.; Gulyas, B., Nanoparticle Functionalization and Its Potentials for Molecular Imaging. *Adv Sci (Weinh)* **2017**, *4* (3), 1600279.
19. Guerrini, L.; Alvarez-Puebla, R. A.; Pazos-Perez, N., Surface Modifications of Nanoparticles for Stability in Biological Fluids. *Materials (Basel)* **2018**, *11* (7).
20. Generalova, A. N.; Kochneva, I. K.; Khaydukov, E. V.; Semchishen, V.A.; Guller, A. E.; Nechaev, A. V.; Shekhter, A. B.; Zubov, V. P.; Zvyagin, A. V.; Deyev, S. M., Submicron polyacrolein particles in situ embedded with upconversion nanoparticles for bioassay. *Nanoscale* **2015**, *7* (5), 1709-17.
21. Gomes, M. C.; Cunha, A.; Trindade, T.; Tome, J. P. C., The role of surface functionalization of silica nanoparticles for bioimaging. *J. Innov. Opt. Health Sci.* **2016**, *9* (4), 16.
22. Dogra, P.; Adolphi, N. L.; Wang, Z. H.; Lin, Y. S.; Butler, K. S.; Durfee, P. N.; Croissant, J. G.; Noureddine, A.; Coker, E. N.; Bearer, E. L.; Cristini, V.; Brinker, C. J., Establishing the effects of mesoporous silica nanoparticle properties on in vivo disposition using imaging-based pharmacokinetics. *Nature Communications* **2018**, *9*.

23. Cho, E. C.; Xie, J.; Wurm, P. A.; Xia, Y., Understanding the Role of Surface Charges in Cellular Adsorption versus Internalization by Selectively Removing Gold Nanoparticles on the Cell Surface with a I<sub>2</sub>/KI Etchant. *Nano Letters* **2009**, *9* (3), 1080-1084.
24. Kobayashi, H.; Ogawa, M.; Alford, R.; Choyke, P.; Urano, Y., New Strategies for Fluorescent Probe Design in Medical Diagnostic Imaging. *Chemical reviews* **2009**, *110*, 2620-40.
25. Santra, S.; Zhang, P.; Wang, K.; Tapeç, R.; Tan, W., Conjugation of Biomolecules with Luminophore-Doped Silica Nanoparticles for Photostable Biomarkers. *Analytical chemistry* **2001**, *73*, 4988-93.
26. Guo, B. L.; Sui, B. D.; Wang, X. Y.; Wei, Y. Y.; Huang, J.; Chen, J.; Wu, S. X.; Li, Y. Q.; Wang, Y. Y.; Yang, Y. L., Significant changes in mitochondrial distribution in different pain models of mice. *Mitochondrion* **2013**, *13* (4), 292-7.
27. Qu, Q.; Ma, X.; Zhao, Y., Anticancer Effect of alpha-Tocopheryl Succinate Delivered by Mitochondria-Targeted Mesoporous Silica Nanoparticles. *ACS Appl Mater Interfaces* **2016**, *8* (50), 34261-34269.
28. He, Q.; Zhang, Z.; Gao, Y.; Shi, J.; Li, Y., Intracellular localization and cytotoxicity of spherical mesoporous silica nano- and microparticles. *Small* **2009**, *5* (23), 2722-9.
29. Xue, Z., Silica nanoparticle is a possible safe carrier for gene therapy. *Chinese Science Bulletin* **2005**, *50* (20).
30. Wang, Z.-R.; Cui, Y.; Qiu, Z.-Y., Biomimetic Mineralized Collagen Biocompatibility. In *Mineralized Collagen Bone Graft Substitutes*, **2019**; pp 61-98.
31. Kim, I. Y.; Joachim, E.; Choi, H.; Kim, K., Toxicity of silica nanoparticles depends on size, dose, and cell type. *Nanomedicine* **2015**, *11* (6), 1407-16.
32. Annika Mareike Gramatke, I. L. H., Size and Cell Type Dependent Uptake of Silica Nanoparticles. *Journal of Nanomedicine & Nanotechnology* **2014**, *05* (06).
33. Nowak, J. S.; Mehn, D.; Nativo, P.; Garcia, C. P.; Gioria, S.; Ojea-Jimenez, I.; Gilliland, D.; Rossi, F., Silica nanoparticle uptake induces survival mechanism in A549 cells by the activation of autophagy but not apoptosis. *Toxicol Lett* **2014**, *224* (1), 84-92.
34. Kim, J. Y.; Park, J. H.; Kim, M.; Jeong, H.; Hong, J.; Chuck, R. S.; Park, C. Y., Safety of Nonporous Silica Nanoparticles in Human Corneal Endothelial Cells. *Sci Rep* **2017**, *7* (1), 14566.
35. Xia, Y.; Li, M.; Peng, T.; Zhang, W.; Xiong, J.; Hu, Q.; Song, Z.; Zheng, Q., In vitro cytotoxicity of fluorescent silica nanoparticles hybridized

- with aggregation-induced emission luminogens for living cell imaging. *Int J Mol Sci* **2013**, *14* (1), 1080-92.
36. Lin, W.; Huang, Y. W.; Zhou, X. D.; Ma, Y., In vitro toxicity of silica nanoparticles in human lung cancer cells. *Toxicol Appl Pharmacol* **2006**, *217* (3), 252-9.
  37. Xu, X.; Zhang, K.; Zhao, L.; Wang, D.; Bu, W.; Zheng, C.; Sun, H., Characteristics of three sizes of silica nanoparticles in the osteoblastic cell line, MC3T3-E1. *RSC Adv.* **2014**, *4* (87), 46481-46487.
  38. Gomes, M. C.; Cunha, A.; Trindade, T.; Tome, J. P. C., The role of surface functionalization of silica nanoparticles for bioimaging. *J. Innov. Opt. Health Sci.* **2016**, *9* (4), 16.
  39. Ogawa, T.; Aoyagi, S.; Miyasaka, T.; Sakai, K., Fluorescence enhancement of fluorescein isothiocyanate-labeled protein a caused by affinity binding with immunoglobulin g in bovine plasma. *Sensors (Basel)* **2009**, *9* (10), 8271-7.
  40. Alluska: Fluorescence Filters for Microscopy and Imaging. <https://www.alluxa.com/optical-filter-applications/fluorescence-filters-microscopy-imaging/> (accessed May 14, **2018**).
  41. Gao, Z.; Hao, Y.; Zheng, M.; Chen, Y., A fluorescent dye with large Stokes shift and high stability: synthesis and application to live cell imaging. *RSC Advances* **2017**, *7* (13), 7604-7609.
  42. Dogra, P.; Adolphi, N. L.; Wang, Z. H.; Lin, Y. S.; Butler, K. S.; Durfee, P. N.; Croissant, J. G.; Noureddine, A.; Coker, E. N.; Bearer, E. L.; Cristini, V.; Brinker, C. J., Establishing the effects of mesoporous silica nanoparticle properties on in vivo disposition using imaging-based pharmacokinetics. *Nature Communications* **2018**, *9*.
  43. Hassan, P. A.; Rana, S.; Verma, G., Making sense of Brownian motion: colloid characterization by dynamic light scattering. *Langmuir* **2015**, *31* (1), 3-12.
  44. Madushani, S., Nature. Ozone Layer and Us. <https://www.fabpretty.com/nature/ozone-layer-and-us/> (accessed Apr 18, **2013**).
  45. George, K. M.; Ruthenburg, T. C.; Smith, J.; Yu, L.; Zhang, Q.; Anastasio, C.; Dillner, A. M., FT-IR quantification of the carbonyl functional group in aqueous-phase secondary organic aerosol from phenols. *Atmospheric Environment* **2015**, *100*, 230-237.
  46. Chen, X.; Zheng, B.; Liu, H., Optical and digital microscopic imaging techniques and applications in pathology. *Anal Cell Pathol (Amst)* **2011**, *34* (1-2), 5-18

47. Crawford, B.J., Liley, C.R.W., *J. Phys. E* **3**, 461 (1970).
48. Yang, J.; Bai, J.; Liu, M.; Chen, Y.; Wang, S.; Yang, Q., Determination of Phosphorus in Soil by ICP-OES Using an Improved Standard Addition Method. *J Anal Methods Chem* **2018**, *2018*, 1324751.
49. Sarkar, K.; Salinas, Y.; Campos, I.; Martínez-Máñez, R.; Marcos, M. D.; Sancenón, F.; Amorós, P., Organic-Inorganic Hybrid Mesoporous Materials as Regenerable Sensing Systems for the Recognition of Nitroaromatic Explosives. *ChemPlusChem* **2013**, *78* (7), 684-694.
50. Vanblaaderen, A.; Vrij, A., SYNTHESIS AND CHARACTERIZATION OF MONODISPERSE COLLOIDAL ORGANO-SILICA SPHERES. *Journal of Colloid and Interface Science* **1993**, *156* (1), 1-18.
51. Townson, J. L.; Lin, Y. S.; Agola, J. O.; Carnes, E. C.; Leong, H. S.; Lewis, J. D.; Haynes, C. L.; Brinker, C. J., Re-examining the size/charge paradigm: differing in vivo characteristics of size- and charge-matched mesoporous silica nanoparticles. *J Am Chem Soc* **2013**, *135* (43), 16030-3.
52. Dasog, M.; De los Reyes, G. B.; Titova, L. V.; Hegmann, F. A.; Veinot, J. G. C., Size vs Surface: Tuning the Photoluminescence of Freestanding Silicon Nanocrystals Across the Visible Spectrum via Surface Groups. *Acs Nano* **2014**, *8* (9), 9636-9648.
53. American Type Culture Collection. A549 (ATCC<sup>®</sup> CCL-185<sup>™</sup>) and BEAS-2B (ATCC<sup>®</sup> CRL-9609<sup>™</sup>). <https://www.lgcstandards-atcc.org> (accessed **2016**).
54. Qiao, L.; Farrell, G. C., The effects of cell density, attachment substratum and dexamethasone on spontaneous apoptosis of rat hepatocytes in primary culture. *In vitro cellular & developmental biology. Animal* **1999**, *35* (7), 417-24.
55. World Health Organization. International Agency for Research on Cancer. <http://gco.iarc.fr/today/data/factsheets/populations/792-turkey-fact-sheets.pdf> (accessed **2018**).
56. Bray, F.; Ferlay, J.; Soerjomataram, I.; Siegel, RL.; Torre, LA.; Jemal, A., Global Cancer Statistics. <https://www.wcrf.org/dietandcancer/cancer-trends/worldwide-cancer-data> (accessed **2018**).
57. Mosmann, T., Rapid colorimetric assay for cellular growth and survival: application to proliferation and cytotoxicity assays. *J Immunol Methods* **1983**, *65* (1-2), 55-63.
58. Brand, M. D., Orr, A. L., Perevoshchikova, I. V., & Quinlan, C. L., The role of mitochondrial function and cellular bioenergetics in ageing and disease. *The British journal of dermatology* **2013**, *169* Suppl 2(0 2), 1–8.

59. Kim, S. O.; Kim, J.; Okajima, T.; Cho, N. J., Mechanical properties of paraformaldehyde-treated individual cells investigated by atomic force microscopy and scanning ion conductance microscopy. *Nano Converg* **2017**, *4* (1), 5.
60. Hobro, A. J.; Smith, N. I., An evaluation of fixation methods: Spatial and compositional cellular changes observed by Raman imaging. *Vibrational Spectroscopy* **2017**, *91*, 31-45.
61. Cottet-Rousselle, C.; Ronot, X.; Leverve, X.; Mayol, J. F., Cytometric assessment of mitochondria using fluorescent probes. *Cytometry A* **2011**, *79* (6), 405-25.
62. Zorova, L. D.; Popkov, V. A.; Plotnikov, E. Y.; Silachev, D. N.; Pevzner, I. B.; Jankauskas, S. S.; Babenko, V. A.; Zorov, S. D.; Balakireva, A. V.; Juhaszova, M.; Sollott, S. J.; Zorov, D. B., Mitochondrial membrane potential. *Anal Biochem* **2018**, *552*, 50-59.
63. Chakrabarti, L.; Mathew, A.; Li, L.; Han, S.; Klover, J.; Albanetti, T.; Hawley-Nelson, P., Mitochondrial membrane potential identifies cells with high recombinant protein productivity. *J Immunol Methods* **2019**, *464*, 31-39.
64. McDorman, K. S.; Chan, C.; Rojko, J.; Satterwhite, C. M.; Morrison, J. P., Special Techniques in Toxicologic Pathology. In *Haschek and Rousseaux's Handbook of Toxicologic Pathology*, **2013**; pp 175-214.
65. Fellers, J. T.; Davidson, W. M., National High Magnetic Field Laboratory. Introduction to Confocal Microscopy. <https://micro.magnet.fsu.edu/primer/techniques/confocalintroduction.html>
66. Jonkman, J.; Brown, C. M., Any Way You Slice It-A Comparison of Confocal Microscopy Techniques. *J Biomol Tech* **2015**, *26* (2), 54-65.
67. Davidson, W. M.; National High Magnetic Field Laboratory. <http://zeiss-campus.magnet.fsu.edu/articles/spinningdisk/introduction.html>
68. Aaron, J. S.; Taylor, A. B.; Chew, T. L., Image co-localization - co-occurrence versus correlation. *J Cell Sci* **2018**, *131* (3).
69. Kusaczuk, M.; Kretowski, R.; Naumowicz, M.; Stypulkowska, A.; Cechowska-Pasko, M., Silica nanoparticle-induced oxidative stress and mitochondrial damage is followed by activation of intrinsic apoptosis pathway in glioblastoma cells. *Int J Nanomedicine* **2018**, *13*, 2279-2294.
70. Wang, F.; Gao, F.; Lan, M.; Yuan, H.; Huang, Y.; Liu, J., Oxidative stress contributes to silica nanoparticle-induced cytotoxicity in human embryonic kidney cells. *Toxicol In Vitro* **2009**, *23* (5), 808-15.

71. Battogtokh, G.; Cho, Y. Y.; Lee, J. Y.; Lee, H. S.; Kang, H. C., Mitochondrial-Targeting Anticancer Agent Conjugates and Nanocarrier Systems for Cancer Treatment. *Front Pharmacol* **2018**, *9*, 922.
72. Heerdt, B. G.; Houston, M. A.; Augenlicht, L. H., The intrinsic mitochondrial membrane potential of colonic carcinoma cells is linked to the probability of tumor progression. *Cancer Res* **2005**, *65* (21), 9861-7.
73. McDonald, J. H.; Dunn, K. W., Statistical tests for measures of colocalization in biological microscopy. *J Microsc* **2013**, *252* (3), 295-302.
74. Selvaraj, V.; Bodapati, S.; Murray, E.; Rice, K. M.; Winston, N.; Shokuhfar, T.; Zhao, Y.; Blough, E., Cytotoxicity and genotoxicity caused by yttrium oxide nanoparticles in HEK293 cells. *Int J Nanomedicine* **2014**, *9*, 1379-91.
75. Hussain, S., Measurement of Nanoparticle-Induced Mitochondrial Membrane Potential Alterations. *Methods Mol Biol* **2019**, *1894*, 123-131.